Role of a "Magic" Methyl: 2′-Deoxy-2′-α-F-2′-β-C-methyl Pyrimidine Nucleotides Modulate RNA Interference Activity through Synergy with 5′-Phosphate Mimics and Mitigation of Off-Target Effects

Dale C. Guenther, Shohei Mori, Shigeo Matsuda, Jason A. Gilbert, Jennifer L. S. Willoughby, Sarah Hyde, Anna Bisbe, Yongfeng Jiang, Saket Agarwal, Mimouna Madaoui, Maja M. Janas, Klaus Charisse, Martin A. Maier, Martin Egli, and Muthiah Manoharan*

ACCESS | Metrics & More | Article Recommendations | Supporting Information

ABSTRACT: Although 2′-deoxy-2′-α-F-2′-β-C-methyl (2′-F/Me) uridine nucleoside derivatives are a successful class of antiviral drugs, this modification had not been studied in oligonucleotides. Herein, we demonstrate the facile synthesis of 2′-F/Me-modified pyrimidine phosphoramidites and their subsequent incorporation into oligonucleotides. Despite the C3′-*endo* preorganization of the parent nucleoside, a single incorporation into RNA or DNA resulted in significant thermal destabilization of a duplex due to unfavorable enthalpy, likely resulting from steric effects. When located at the terminus of an oligonucleotide, the 2′-F/Me modification imparted more resistance to degradation than the corresponding 2′-fluoro nucleotides. Small interfering RNAs (siRNAs) modified at certain positions with 2′-F/Me had similar or better silencing activity than the parent siRNAs when delivered via a lipid nanoparticle formulation or as a triantennary *N*-acetylgalactosamine conjugate in cells and in mice. Modification in the seed region of the antisense strand at position 6 or 7 resulted in an activity equivalent to the parent in mice. Additionally, placement of the antisense strand at position 7 mitigated seed-based off-target effects in cell-based assays. When the 2′-F/Me modification was combined with 5′-vinyl phosphonate, both *E* and *Z* isomers had silencing activity comparable to the parent. In combination with other 2′-modifications such as 2′-*O*-methyl, the *Z* isomer is detrimental to silencing activity. Presumably, the equivalence of 5′-vinyl phosphonate isomers in the context of 2′-F/Me is driven by the steric and conformational features of the *C*-methyl-containing sugar ring. These data indicate that 2′-F/Me nucleotides are promising tools for nucleic acid-based therapeutic applications to increase potency, duration, and safety.
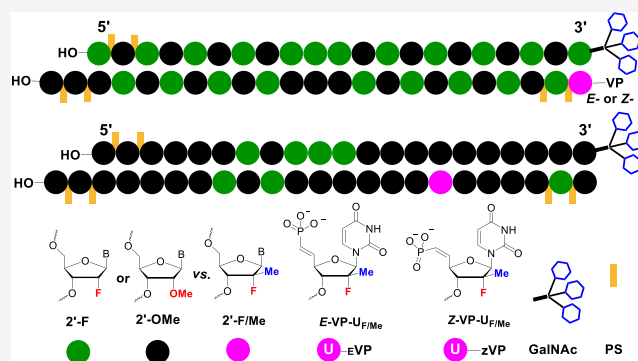
INTRODUCTION

RNA interference (RNAi) is a post-transcriptional pathway for gene regulation mediated by small interfering RNAs (siRNAs).[1−3] siRNAs, loaded onto Argonaute 2 (Ago2), the catalytic component of the RNA-induced silencing complex (RISC), target complementary mRNAs for degradation, thereby reducing the expression of the encoded protein.[4] Synthetic siRNAs are powerful tools for fundamental research and are used clinically for the treatment of multiple diseases including hereditary transthyretin-mediated amyloidosis, acute hepatic porphyrias, primary hyperoxaluria type 1, and heterozygous familial hypercholesterolemia.[5−19] For liver-specific delivery, siRNAs are formulated in lipid nanoparticles (LNPs)[13] or conjugated with a triantennary *N*-acetylgalactos-amine (GalNAc) ligand, which results in hepatocyte-specific uptake via the asialoglycoprotein receptor.[20] Clinically used siRNAs are also chemically modified to improve potency, increase metabolic stability, avoid immune responses, and

mitigate off-target effects.[21−23] Ribose modifications currently used in clinically approved siRNAs are 2′-deoxy, 2′-fluoro (2′-F), and 2′-*O*-methyl (2′-OMe). These modifications provide sufficient specificity and metabolic stability when combined with phosphorothioate (PS) linkages at 5′ and 3′ termini to result in excellent safety and efficacy profiles in patients.

The chemical modifications 2′-F and 2′-OMe are pre-organized into an RNA-like C3′-*endo* conformation, resulting in enhanced binding to RNA, favorable binding to Ago2, and increased resistance toward nuclease degradation relative to siRNAs with the parent ribonucleotide.[24,25] We reasoned that
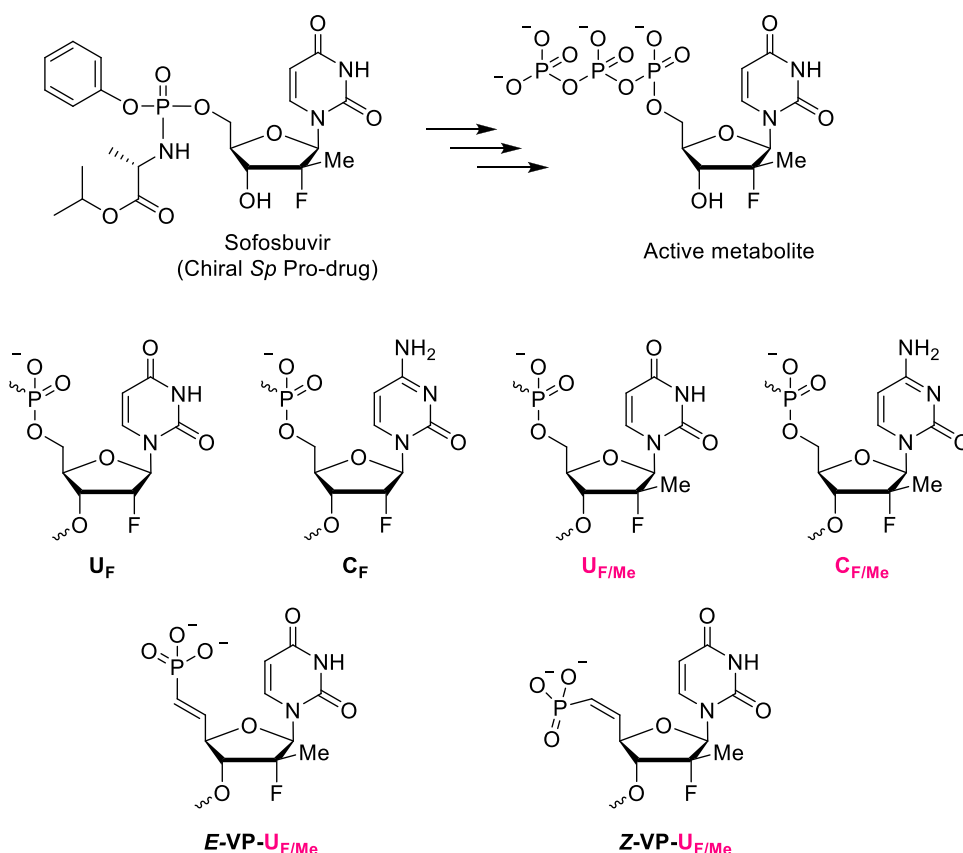
Figure 1. Structures of the antiviral HCV drug sofosbuvir and the active metabolite, which inspired the modifications 2′-F/Me uridine ($U_{F/Me}$) and cytidine ($C_{F/Me}$) and the corresponding 5′-VP isomers of $U_{F/Me}$ studied herein.

other nucleosides preorganized into the C3′-*endo* conformation might be used to optimize siRNA activity. The C3′-*endo* conformation is favored upon alkylation of the sugar as in 2′-deoxy-2′-α-C-methyl thymidine.[26−28] In the 2′-C-methyl-uridine nucleoside, the 2′-C-methyl substituent adopts a pseudoequatorial conformation due to steric interactions, the C2′−OH group has a stabilizing O4′−O2′ gauche effect, the C-5′ side chain is pseudoequatorial, and the base is pseudoaxial, satisfying the weak anomeric effect.[12,29] Sugar-alkylated nucleosides have been developed for use as antiviral agents against the hepatitis C virus (HCV).[25,30−32] Sofosbuvir, the first ribonucleotide analogue inhibitor to receive FDA approval for treatment of HCV,[33−38] is a prodrug of 2′-deoxy-2′-α-C-F-2′-β-C-Me (2′-F/Me) uridine triphosphate (Figure 1). The 2′-F/Me uridine triphosphate does not act as a substrate for human mitochondrial polymerases, likely due to the steric bulk around the 2′ position.[39]

The C3′-*endo* sugar conformation of 2′-F/Me nucleotide, lack of mitochondrial toxicity, and metabolic stability render it an interesting modification for RNAi applications. The lack of mitochondrial toxicity is particularly important for any chemical modification used for therapeutic oligonucleotides to avoid potential safety risks arising from nucleotide metabolites.[40] In RNAi, a nonhydrolyzable, metabolically stable 5′ phosphate mimic such as (*E*)-vinyl phosphonate (VP) at the 5′ terminus of the antisense strand enables selective recognition of this strand over the sense strand by the MID domain of Ago2, resulting in improved potency.[22,41−47] Hybridization-based off-target effects can be mitigated by mechanisms that ensure proper strand selection or through the

judicious incorporation of destabilizing modifications like glycol nucleic acids (GNA).[48−56]

Herein, we describe the synthesis of 2′-F/Me-pyrimidine phosphoramidites and the effects of this modification on duplex thermal stability, resistance toward exonuclease degradation, and on- and off-target activity of siRNAs. Our observations were rationalized using molecular modeling of appropriate nucleic acid−protein interactions. Our findings indicate that further evaluation of this modification in the context of RNA-based therapeutics is warranted.

■ RESULTS AND DISCUSSION

Synthesis of RNA Oligonucleotides Containing 2′-F/Me-Pyrimidine. The 2′-F/Me-pyrimidine phosphoramidites (**3** and **6**) were synthesized from the corresponding commercially available nucleosides (**1** and **4**) using standard nucleoside protection with a 4,4′-dimethoxytrityl group at the 5′ position, a benzoyl group at the exocyclic amine of cytosine base, and phosphitylation (Scheme 1). The bis-pivaloyloxy-methyl vinyl phosphonate **7** was synthesized using methods developed in our laboratories for other nucleosides.[22,41−47] The mixture of diastereomers ($E/Z \approx 5/1$) was separated into pure isomers **8** and **9** after the desilylation of the 3′-hydroxy group. The 3′-hydroxy groups of these nucleoside monomers were converted to the phosphoramidite forms (Scheme 1; see the Supporting Information for details). The phosphoramidite building blocks were site-specifically incorporated into oligonucleotides using an automated synthesizer. Cleavage from the solid support and subsequent deprotection of the synthesized oligonucleotides were performed under standard

Scheme 1. Synthesis of 2′-F/Me-Pyrimidine Building Blocks
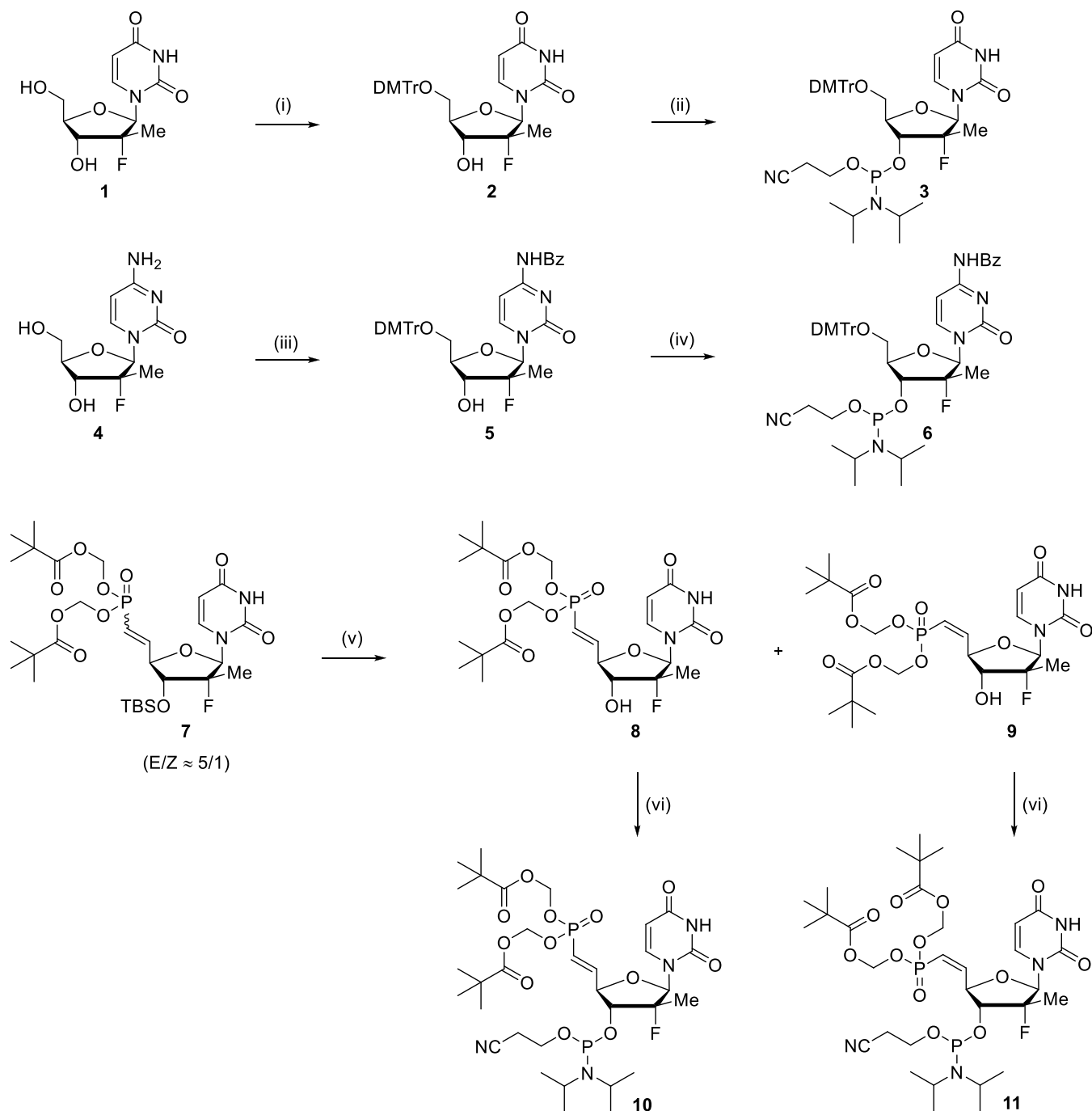
[a]Reagents and conditions: (i) DMTrCl/pyridine, room temperature, 16 h, 61%; (ii) 2-cyanoethyl *N,N*-diisopropylchlorophosphoramidite/DIPEA/ CH₂Cl₂, room temperature, 16 h, 90%; (iii) Bz₂O/*N,N*-dimethylformamide (DMF), room temperature, 24 h, then DMTrCl/pyridine, room temperature, 16 h, 74%; (iv) 2-cyanoethyl *N,N,N′,N′*-tetraisopropylphosphorodiamidite/4,5-dicyanoimidazole/CH₂Cl₂, room temperature, 16 h, 95%; (v) HCOOH/H₂O, 40 °C, 16 h, **8**: 60%, **9**: 12%; (vi) 2-cyanoethyl *N,N,N′,N′*-tetraisopropylphosphorodiamidite/5-ethylthio-2*H*-tetrazole/ CH₃CN, room temperature, 2 h, **10**: 74%, **11**: 75%.

conditions using ammonium hydroxide solution. The crude oligonucleotides were purified by high-performance liquid chromatography (HPLC) and characterized by liquid chromatography-mass spectrometry (LC-MS) (Table S1; see the Supporting Information for details).

Thermodynamic Stabilities of Duplexes Containing RNA Strands Modified with 2′-F/Me-Pyrimidine Nucleotides. Melting temperatures (T_m) and thermodynamic

parameters of hybridization of 12-mer RNA duplexes containing a single, centrally located 2′-F or 2′-F/Me modification were evaluated (Table 1). Duplexes containing 2′-F-modified U or C (U_F and C_F, respectively) had similar or slightly increased T_m values compared to the unmodified RNA duplex (**ON3:ON2** and **ON5:ON2** vs **ON1:ON2**). The incorporation of 2′-F/Me-modified nucleotides ($U_{F/Me}$ and $C_{F/Me}$) dramatically reduced the T_m by about 15 °C relative to

Table 1. Thermal Denaturation Temperatures and Thermodynamic Parameters of Duplexes with an RNA Strand Containing 2′-F or 2′-F/Me-Pyrimidine[a]

ON	sequence	T_m (°C)	ΔT_m (°C)	ΔG_{310} (kJ/mol)	ΔH (kJ/mol)	$T_{310}\Delta S$ (kJ/mol)
1	5′-r(UACAGUCUAUGU)	54.1		−58 ± 0	−453 ± 6	−395 ± 6
2	3′-r(AUGUCAGAUACA)					
3	5′-r(UACAGU$_F$CUAUGU)	53.9	−0.2	−60 ± 0	−449 ± 4	−388 ± 3
2	3′-r(AUGUCAGAUACA)					
4	5′-r(UACAGU$_{F/Me}$CUAUGU)	39.1	−15.0	−38 ± 0	−343 ± 6	−304 ± 6
2	3′-r(AUGUCAGAUACA)					
5	5′-r(UACAGUC$_F$UAUGU)	55.1	+1.1	−61 ± 0	−444 ± 3	−383 ± 3
2	3′-r(AUGUCAGAUACA)					
6	5′-r(UACAGUC$_{F/Me}$UAUGU)	38.3	−15.8	−38 ± 1	−347 ± 7	−309 ± 7
2	3′-r(AUGUCAGAUACA)					

[a]The absorbances of hybridized duplexes (2.5 μM) at 260 nm were determined as a function of temperature in phosphate-buffered saline (PBS; 137 mM NaCl, 2.7 mM KCl, 10 mM Na$_2$HPO$_4$, 1.8 mM KH$_2$PO$_4$, pH 7.4). The T_m was determined as the maximum of the first derivative of the melting curve. Values are reported as the average of two independent experiments. ΔT_m was calculated with respect to the unmodified RNA duplex. Thermodynamic parameters are an average of six determinations using the Varian Cary Bio-300 built-in software, with a standard deviation reported.

Table 2. Thermal Denaturation Temperatures of Modified Duplexes Containing a Single Mismatch[a]

			ΔT_m (°C)					
			3′-AUGUC**B**GAUACA			3′-AUGUCA**B**AUACA		
	modified strand	T_m (°C)						
		ON2	ON7 G	ON8 U	ON9 C	ON10 C	ON11 U	ON12 A
ON1	5′-UACAGUCUAUGU	61.6	−1.5	−11.4	−11.9	−21.1	−18.6	−18.5
ON3	5′-UACAGU$_F$CUAUGU	62.2	−2.0	−12.4	−12.9	−21.1	−19.5	−18.9
ON4	5′-UACAGU$_{F/Me}$CUAUGU	47.1	−2.6	−5.1	−8.0	−16.4	−15.8	−12.7
ON5	5′-UACAGUC$_F$UAUGU	63.1	−2.6	−12.1	−12.0	−21.9	−19.8	−19.7
ON6	5′-UACAGUC$_{F/Me}$UAUGU	45.2	0.0	−9.9	−13.9	−15.7	−13.3	−13.1

[a]T_m was measured by monitoring the absorbance of hybridized duplexes (2.5 μM) with increasing temperature in high-salt PBS. ΔT_m is calculated with respect to the corresponding fully complementary duplexes.

the unmodified RNA duplex. There seemed to be little sequence dependence of this destabilization, as it was observed for both U$_{F/Me}$:A and C$_{F/Me}$:G base pairs flanked by G:C or U:A base pairs in **ON4:ON2** and **ON6:ON2**, respectively. This pattern of decreased thermal stability was also observed in the contexts of RNA:DNA and DNA:DNA duplexes, where even in high-salt phosphate-buffered saline (high-salt PBS; 1.14 M NaCl, 2.7 mM KCl, 10 mM Na$_2$HPO$_4$, 1.8 mM KH$_2$PO$_4$, pH 7.4) a clear transition was not apparent (Table S2). In particular, the shape of the melting curves for duplexes containing U$_{F/Me}$ and the complementary DNA strand were quite broad.

The thermodynamic parameters were obtained using the Van't Hoff method based on the hyperchromicity of melting curves (Table 1). The duplexes formed from a modified RNA strand with a complementary RNA have relatively sharp transitions (Figure S1), thus supporting the assumption of a two-state model.[57] The changes in the Gibbs free energy of hybridization closely resemble the trends seen with T_m values that showed that 2′-F/Me modifications significantly reduced the thermal stability of the duplex. Both RNA and 2′-F-modified duplexes were thermodynamically favorable with ΔG_{310} values of approximately −60 kJ/mol, whereas those formed from 2′-F/Me-modified strands were less favorable by about 20 kJ/mol (compare **ON1:ON2** vs **ON4:ON2** and **ON6:ON2**). The reduced stability of the 2′-F/Me-modified duplex appears to be due to unfavorable enthalpic contributions, which are largely compensated by favorable entropic contributions. Even though U$_{F/Me}$ and C$_{F/Me}$ adopt C3′-endo sugar puckers, which are preorganized for binding to RNA,

destabilization suggests that other interactions (e.g., base pairing, stacking) that result in favorable enthalpic contributions are compromised.

Mismatch Discrimination by RNA Oligonucleotides Modified with 2′-F/Me-Pyrimidine Nucleotides. Next, the ability to thermally discriminate a single-base mismatch in a duplex containing a modified nucleotide was evaluated (Table 2). Duplexes were formed between RNA strands containing either U$_F$ (**ON3**) or U$_{F/Me}$ (**ON4**) and a fully complementary RNA strand, with an RNA strand with a single mismatch with the uridine derivative (**ON7**, **ON8**, or **ON9**), or with an RNA strand with a mismatch on the 3′ side of the modified nucleotide (**ON10**, **ON11**, or **ON12**). We also evaluated duplexes formed between RNA strands containing either C$_F$ (**ON5**) or C$_{F/Me}$ (**ON6**) with **ON10**, **ON11**, or **ON12**, resulting in mismatches to the 3′ side of the modified nucleotide, or duplexes formed with **ON7**, **ON8**, or **ON9**, resulting in mismatches to the 5′ side of the modified nucleotide. Due to the lower melting temperature caused by the mismatches, these duplexes were evaluated in a high-salt buffer, where both canonical RNA duplexes and those containing a 2′-F nucleotide exhibited similar and excellent thermal discrimination, regardless of the proximity of the mismatch to the modification (Table 2).

When U$_{F/Me}$ was located directly opposite of guanosine (**ON4:ON7**), the discrimination was increased by approximately 1 °C for the G:U wobble compared to unmodified RNA (**ON4:ON7** vs **ON1:ON7**). For the other mismatches, we observed a lower T_m reduction compared to unmodified RNA. Interestingly, this reduced discrimination was propa-
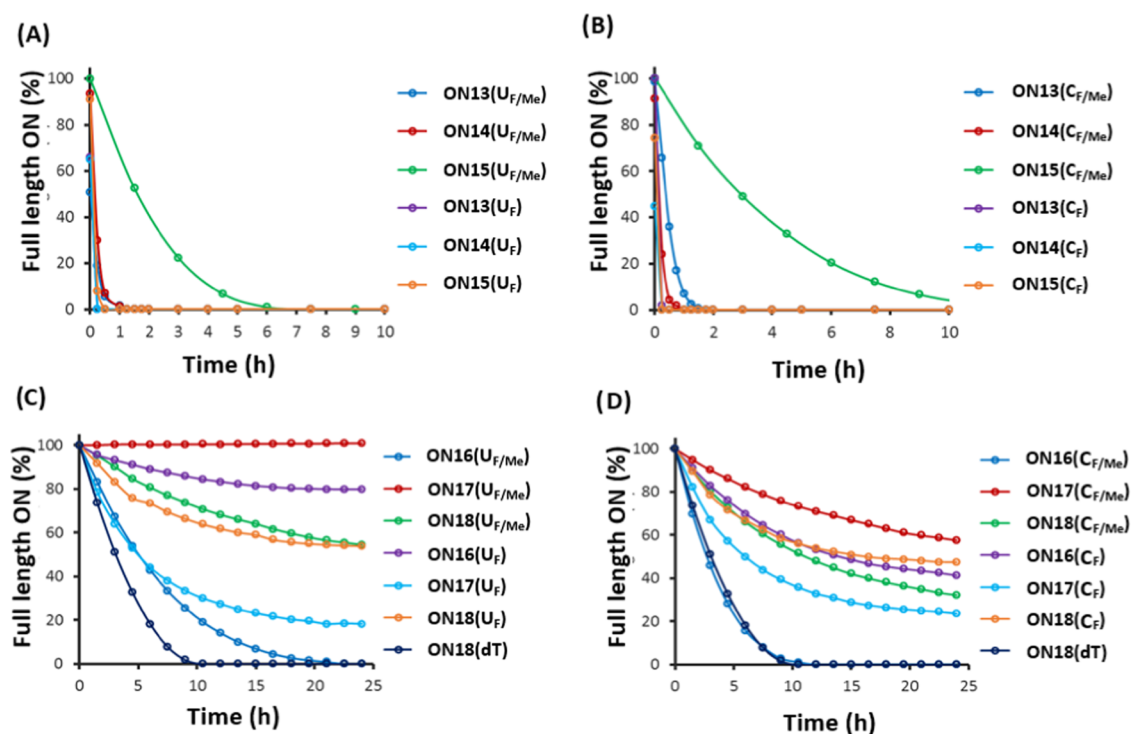
Figure 2. Nuclease degradation profiles of 3′-modified oligonucleotides in the presence of 3′ exonuclease. Plots of full-length oligonucleotide versus time for (A) **ON13** ($dT_{19}X$-3′), **ON14** ($dT_{18}XdT$), and **ON15** ($dT_{18}X_2$), where X is either $U_{Me/F}$ or U_F; (B) **ON13** ($dT_{19}X$-3′), **ON14** ($dT_{18}XdT$), and **ON15** ($dT_{18}X_2$), where X is either $C_{Me/F}$ or C_F; (C) **ON16** ($dT_{19}\bullet X$-3′), **ON17** ($dT_{18}\bullet X\bullet dT$-3′), and **ON18** ($dT_{18}X\bullet X$-3′), where "•" indicates a PS linkage and X is either $U_{Me/F}$ or U_F; and (D) **ON16** ($dT_{19}X$-3′), **ON17** ($dT_{18}X\bullet dT$-3′), and **ON18** ($dT_{18}X\bullet X$-3′), where "•" indicates a PS linkage and X is either $C_{Me/F}$ or C_F. Oligonucleotides (0.1 mg/mL) were incubated with 150 mU/mL SVPD in 50 mM Tris, pH 7.2, and 10 mM $MgCl_2$, and the full-length product was monitored via IEX-HPLC.

Table 3. Half-Lives of Oligonucleotides Incubated with 3′ Exonuclease SVPD[a]

	$t_{1/2}$ in the presence of 3′-exonuclease (h)					
X =	ON13(X) $dT_{19}X$	ON14(X) $dT_{18}XdT$	ON15(X) $dT_{18}XX$	ON16(X) $dT_{19}\bullet X$	ON17(X) $dT_{18}X\bullet dT$	ON18(X) $dT_{18}X\bullet X$
U_F	<0.2	<0.2	<0.2	79	10	29
$U_{F/Me}$	0.2	0.2	0.9	3.2	no deg.	27
C_F	<0.2	<0.2	<0.2	19	12	24
$C_{F/Me}$	0.6	<0.2	2.0	1.6	31	15

[a]Half-lives were determined by plotting the percent full-length oligonucleotide vs time and fitting to the exponential decay function. For experimental conditions, see Figure 2. PS linkage, •; no deg., no degradation observed within 24 h.

gated to the 3′-adjacent base pair (e.g., **ON4:ON10**, **ON4:ON11**, **ON4:ON12**), suggesting that a local distortion caused by the modification increases the tolerance for mismatches nearby. $C_{F/Me}$ reduced the thermal discrimination of a mismatched nucleobase located directly across from the modified nucleotide (e.g., **ON6:ON10**, **ON6:ON11**, **ON6:ON12**) by about 5 °C compared to unmodified RNA. This loss in thermal discrimination was minimal when the mismatch was on the 5′ side (e.g., **ON6:ON7**, **ON6:ON8**, **ON6:ON9**), suggesting that 2′-F/Me-pyrimidines asymmetrically perturb the duplex in the 3′ direction. It is worth noting that even with reduced mismatch discrimination, the remarkably low absolute melting temperatures would likely increase the overall specificity of hybridization at the biologically relevant temperature of 37 °C.

Exonuclease-Mediated Degradation of Oligonucleotides with 2′-F/Me Modifications. To assess the impact of 2′-F/Me modifications on metabolic stability, terminally modified poly-dT oligonucleotides were incubated in the presence of either a 3′- or a 5′-exonuclease. Oligonucleotides with a full phosphodiester (PO) backbone containing a single 2′-F or 2′-F/Me residue at the terminus or the penultimate position (**ON13** or **ON14**, respectively) were degraded within 1 h in the presence of 3′ exonuclease snake venom phosphodiesterase (SVPD; Figure 2). The doubly modified **ON15**($U_{F/Me}$) and **ON15**($C_{F/Me}$) had $t_{1/2}$ values of approximately 1 and 2 h, respectively (Table 3). Oligonucleotides with a single PS linkage at the 3′ end and either $U_{F/Me}$ or $C_{F/Me}$ were more resistant to SVPD-catalyzed degradation than the corresponding 2′-F-modified oligonucleotides, and two 2′-F/Me-pyrimidine nucleotides connected via a PS linkage had an additional stabilizing effect (Figure 2 and Table 3).

The resistance of 5′-modified oligonucleotides toward 5′-exonuclease-mediated degradation with phosphodiesterase II (PDII) was also evaluated (Table 4). For oligonucleotides with full PO backbones (**ON19**), $U_{F/Me}$ was slightly more stabilizing than U_F. For cytidine derivatives, the benefit of 2′-F/Me was striking: Only 25% degradation was observed after 24 h for the oligonucleotide with a single terminal $C_{F/Me}$ modification, whereas the oligonucleotide with the terminal C_F was

Table 4. Half-Lives of Modified Oligonucleotides Incubated with 5′-Exonuclease PD II[a]

	$t_{1/2}$ in the presence of 5′-exonuclease (h)					
X =	(X) ON19 XdT_{19}	(X) ON20 $dTXdT_{18}$	(X) ON21 $XXdT_{18}$	(X) ON22 $X{\bullet}dT_{19}$	(X)ON23 $dT{\bullet}XdT_{18}$	(X) ON24 $X{\bullet}XdT_{18}$
U_F	<0.2	<0.2	<0.2	32	17	43
$U_{F/Me}$	0.9	0.6	1.8	no deg.	50	no deg.
C_F	<0.2	n.d.	0.3	no deg.	n.d.	5.8
$C_{F/Me}$	55	n.d.	260	no deg.	n.d.	no deg.

[a]Half-lives ($t_{1/2}$) were determined by plotting the percent full-length oligonucleotide vs time and fitting to the exponential decay function. For experimental conditions, see Figure 3. n.d., not determined; no deg., no degradation observed within 24 h.

completely degraded within 1 h (**ON19($C_{F/Me}$)** vs **ON19(C_F)**; Figure 3). The addition of a terminal PS linkage (**ON21**) completely stabilized oligonucleotides modified with either $C_{F/Me}$ or C_F against degradation, which could reflect a substrate preference of this particular enzyme, as previously noted.[58] In summary, $U_{F/Me}$ and $C_{F/Me}$ provide better 5′-exonuclease protection than U_F and C_F.

In Vitro RNAi Activity of siRNAs Modified with 2-F/Me Nucleotides. The gene silencing activities of siRNAs with 2′-F/Me modifications targeting three different mRNAs, *Ttr*, *Pten*, and *F7*, were evaluated in cell culture. Modified siRNAs targeting *Ttr* mRNA queried the effect of the 2′-F/Me modification at the 3′ and 5′ termini of the antisense strand (Table 5 and Figure 4A). Evidence indicates that 5′ phosphorylation of the antisense strand is required for efficient

loading of siRNA into RISC and subsequent cleavage of target mRNA by Ago2.[43,45] Modification near the 5′ terminus can impede phosphorylation,[59] so an siRNA with a 2′-F/Me modification at position 1 of the antisense strand was evaluated with either a preinstalled 5′ phosphate group or a 5′-OH (Table 5 and Figure 4A). The efficacy of the parent siRNA, which was modified with 2′-OMe, did not depend on the presence of a phosphate group (compare **si1** vs **si2**). Modification at position 1 with $U_{F/Me}$ in the absence of a preinstalled phosphate (**si3**) resulted in reduced activity, which was largely recovered when the strand was modified with a 5′ phosphate (**si4**) or with 5′-(E)-VP (**si5**). Surprisingly, 5′-(Z)-VP (**si6**) also enhanced RNAi activity to a greater degree than previously observed.[43] Single or double incorporation of $U_{F/Me}$ was well tolerated at the 3′ terminus of the antisense strand, with similar activity as the parent (compare **si7** and **si8** vs **si2**).

Tolerance for modification in the seed region was evaluated for siRNA targeting *Pten* with single incorporation at position 6 or 7 or incorporation at both positions (**si10**, **si11**, and **si12**, respectively, Table 5 and Figure 4B). Modification at position 6 was well tolerated. **si10** had activity similar to that of the parent siRNA (**si9**). Modification at position 7 reduced the IC_{50} to 280 pM, a considerable reduction relative to the 13 pM IC_{50} of the parent. This could be due to the unique structural requirements of Ago2 in this region that necessitates a kink in the siRNA structure.[60] When positions 6 and 7 were modified simultaneously, there was a considerable loss of potency (IC_{50} of 2800 pM).

The siRNA targeting *F7* has several positions that can be modified with 2′-F/Me-pyrimidine nucleotides (Table 5 and
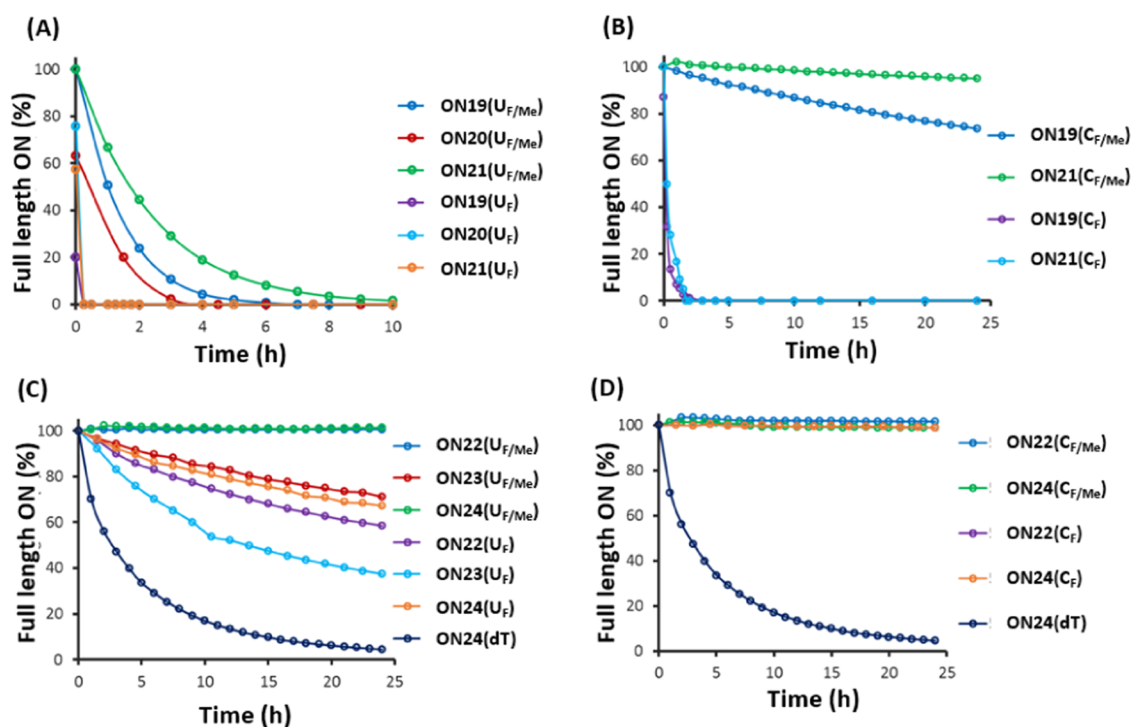
Figure 3. Degradation profiles of 5′-modified oligonucleotides in the presence of 5′-exonuclease. Plots of full-length oligonucleotide versus time for (A) **ON19** (5′-XdT_{19}), **ON20** (5′-$dTXdT_{18}$), and **ON21** (5′-X_2dT_{18}), where X is either $U_{Me/F}$ or U_F; (B) **ON19** (5′-XdT_{19}) and **ON21** (5′-X_2dT_{18}), where X is either $C_{Me/F}$ or C_F; (C) **ON22** (5′-$X{\bullet}dT_{19}$), **ON23** (5′-$dT{\bullet}XdT_{18}$), and **ON24** (5′-$X{\bullet}XdT_{18}$), where "•" indicates a PS linkage and X is either $U_{Me/F}$ or U_F; and (D) **ON22** (5′-$X{\bullet}dT_{19}$), **ON23** (5′-$dT{\bullet}XdT_{18}$), and **ON24** (5′-$X{\bullet}XdT_{18}$), where "•" indicates a PS linkage and X is either $C_{Me/F}$ or C_F. Oligonucleotides (0.1 mg/mL) were incubated with PD II (500 mU/mL) in 50 mM sodium acetate buffer (pH 6.5) with 10 mM $MgCl_2$ and monitored via IEX-HPLC.

Table 5. In Vitro Potency of GalNAc-Conjugated siRNAs With and Without 2′-F/Me Modifications[a]

siRNA	target	strand	sequence (5′ → 3′)	IC$_{50}$ (pM)[b]
si1	*Ttr*	S	A$_F$•a•C$_F$aG$_F$uG$_F$uU$_F$C$_F$U$_F$uG$_F$cU$_F$cU$_F$aU$_F$aA$_F$*	11 ± 4
		AS	u$_•$U$_F$•aU$_F$aG$_F$aG$_F$cA$_F$agaA$_F$cA$_F$cU$_F$gU$_F$u•u•u	
si2	*Ttr*	S	A$_F$•a•C$_F$aG$_F$uG$_F$uU$_F$C$_F$U$_F$uG$_F$cU$_F$cU$_F$aU$_F$aA$_F$*	7 ± 3
		AS	Pu•U$_F$•aU$_F$aG$_F$aG$_F$cA$_F$agaA$_F$cA$_F$cU$_F$gU$_F$u•u•u	
si3	*Ttr*	S	A$_F$•a•C$_F$aG$_F$uG$_F$uU$_F$C$_F$U$_F$uG$_F$cU$_F$cU$_F$aU$_F$aA$_F$*	33 ± 17
		AS	**U$_{F/Me}$**•U$_F$•aU$_F$aG$_F$aG$_F$cA$_F$agaA$_F$cA$_F$cU$_F$gU$_F$u•u•u	
si4	*Ttr*	S	A$_F$•a•C$_F$aG$_F$uG$_F$uU$_F$C$_F$U$_F$uG$_F$cU$_F$cU$_F$aU$_F$aA$_F$*	8 ± 8
		AS	P**U$_{F/Me}$**•U$_F$•aU$_F$aG$_F$aG$_F$cA$_F$agaA$_F$cA$_F$cU$_F$gU$_F$u•u•u	
si5	*Ttr*	S	A$_F$•a•C$_F$aG$_F$uG$_F$uU$_F$C$_F$U$_F$uG$_F$cU$_F$cU$_F$aU$_F$aA$_F$*	2 ± 1
		AS	**VP-U$_{F/Me}$**•U$_F$•aU$_F$aG$_F$aG$_F$cA$_F$agaA$_F$cA$_F$cU$_F$gU$_F$u•u•u	
si6	*Ttr*	S	A$_F$•a•C$_F$aG$_F$uG$_F$uU$_F$C$_F$U$_F$uG$_F$cU$_F$cU$_F$aU$_F$aA$_F$*	11 ± 4
		AS	**zVP-U$_{F/Me}$**•U$_F$•aU$_F$aG$_F$aG$_F$cA$_F$agaA$_F$cA$_F$cU$_F$gU$_F$u•u•u	
si7	*Ttr*	S	A$_F$•a•C$_F$aG$_F$uG$_F$uU$_F$C$_F$U$_F$uG$_F$cU$_F$cU$_F$aU$_F$aA$_F$*	6 ± 4
		AS	Pu•U$_F$•aU$_F$aG$_F$aG$_F$cA$_F$agaA$_F$cA$_F$cU$_F$gU$_F$u•U$_{F/Me}$•u	
si8	*Ttr*	S	A$_F$•a•C$_F$aG$_F$uG$_F$uU$_F$C$_F$U$_F$uG$_F$cU$_F$cU$_F$aU$_F$aA$_F$*	12 ± 5
		AS	Pu•U$_F$•aU$_F$aG$_F$aG$_F$cA$_F$agaA$_F$cA$_F$cU$_F$gU$_F$u•U$_{F/Me}$•U$_{F/Me}$	
si9	*Pten*	S	A$_F$•a•G$_F$aU$_F$gA$_F$uG$_F$U$_F$U$_F$uG$_F$aA$_F$aC$_F$uA$_F$uU$_F$*	13 ± 3
		AS	Pa•A$_F$•uA$_F$gU$_F$U$_F$uC$_F$A$_F$aacA$_F$uC$_F$aU$_F$cU$_F$u•g•u	
si10	*Pten*	S	A$_F$•a•G$_F$aU$_F$gA$_F$uG$_F$U$_F$U$_F$uG$_F$aA$_F$aC$_F$uA$_F$uU$_F$*	35 ± 16
		AS	Pa•A$_F$•uA$_F$g**U$_{F/Me}$**uU$_F$cA$_F$aacA$_F$uC$_F$aU$_F$cU$_F$u•g•u	
si11	*Pten*	S	A$_F$•a•G$_F$aU$_F$gA$_F$uG$_F$U$_F$U$_F$uG$_F$aA$_F$aC$_F$uA$_F$uU$_F$*	280 ± 110
		AS	Pa•A$_F$•uA$_F$gU$_F$U$_F$**U$_{F/Me}$**U$_F$cA$_F$aacA$_F$uC$_F$aU$_F$cU$_F$u•g•u	
si12	*Pten*	S	A$_F$•a•G$_F$aU$_F$gA$_F$uG$_F$U$_F$U$_F$uG$_F$aA$_F$aC$_F$uA$_F$uU$_F$*	2800 ± 1000
		AS	Pa•A$_F$•uA$_F$g**U$_{F/Me}$U$_{F/Me}$**U$_F$cA$_F$aacA$_F$uC$_F$aU$_F$cU$_F$u•g•u	
si13	*F7*	S	C$_F$•a•G$_F$gA$_F$uC$_F$aU$_F$C$_F$U$_F$cA$_F$aG$_F$uC$_F$uU$_F$aA$_F$*	9 ± 16
		AS	u•U$_F$•aA$_F$gA$_F$cU$_F$uG$_F$agaU$_F$gA$_F$uC$_F$cU$_F$g•g•c	
si14	*F7*	S	C$_F$•a•G$_F$gA$_F$uC$_F$aU$_F$C$_F$U$_F$cA$_F$aG$_F$uC$_F$uU$_F$aA$_F$*	0.2 ± 0.4
		AS	Pu•U$_F$•aA$_F$gA$_F$cU$_F$uG$_F$agaU$_F$gA$_F$uC$_F$cU$_F$g•g•c	
si15	*F7*	S	C$_F$•a•G$_F$gA$_F$uC$_F$aU$_F$C$_F$U$_F$cA$_F$aG$_F$uC$_F$uU$_F$aA$_F$*	52 ± 24
		AS	**U$_{F/Me}$**•U$_F$•aA$_F$gA$_F$cU$_F$uG$_F$agaU$_F$gA$_F$uC$_F$cU$_F$g•g•c	
si16	*F7*	S	C$_F$•a•G$_F$gA$_F$uC$_F$aU$_F$C$_F$U$_F$cA$_F$aG$_F$uC$_F$uU$_F$aA$_F$*	10 ± 9
		AS	P**U$_{F/Me}$**•U$_F$•aA$_F$gA$_F$cU$_F$uG$_F$agaU$_F$gA$_F$uC$_F$cU$_F$g•g•c	
si17	*F7*	S	C$_F$•a•G$_F$gA$_F$uC$_F$aU$_F$C$_F$U$_F$cA$_F$aG$_F$uC$_F$uU$_F$aA$_F$*	170 ± 65
		AS	Pu•U$_F$•aA$_F$gA$_F$**C$_{F/Me}$**U$_F$uG$_F$agaU$_F$gA$_F$uC$_F$cU$_F$g•g•c	
si18	*F7*	S	**C$_{F/Me}$**•a•G$_F$gA$_F$uC$_F$aU$_F$C$_F$U$_F$cA$_F$aG$_F$uC$_F$uU$_F$aA$_F$*	6 ± 4
		AS	Pu•U$_F$•aA$_F$gA$_F$cU$_F$uG$_F$agaU$_F$gA$_F$uC$_F$cU$_F$g•g•c	
si19	*Ttr*	S	a•g•uguuC$_F$uU$_F$G$_F$C$_F$ucuauaaaca*	112
		AS	u•G$_F$•uuuauagagcaA$_F$gA$_F$acacu•g•u	
si20	*Ttr*	S	a•g•uguuC$_F$uU$_F$G$_F$C$_F$ucuauaaaca*	60
		AS	u•G$_F$•uuua**U$_{F/Me}$**agagcaA$_F$gA$_F$acacu•g•u	

[a]In vitro potency of fully 2′-modified siRNA targeting indicated mRNAs. Primary mouse hepatocytes were transfected with 10 nM siRNA and 6-fold serial dilutions for *Ttr* of 100 nM siRNA and 5-fold serial dilutions for *Pten* and F7. Target mRNA was quantified using reverse transcription-quantitative polymerase chain reaction (RT-qPCR) after 24 h. For fitted dose-response curves, see Figures S2–S4. 2′-F and 2′-OMe nucleotides are represented as U$_F$ or u, respectively. PS linkage is indicated by "•", 5′-(E)-vinyl phosphonate by VP, 5′-(Z)-vinyl phosphonate by zVP, and the triantennary GalNAc ligand by an asterisk. [b]When given, errors are standard deviations from the mean. Activities of **si19** and **si20** were determined in a dual-luciferase assay; therefore, a standard error cannot be given. For experimental conditions, see Figure 5.

Figure 4C). The siRNA containing a preinstalled 5′ phosphate on the antisense strand had slightly improved activity compared to the parent construct (compare **si14** to **si13**). Similarly, the siRNA with **U$_{F/Me}$** at position 1 of the antisense strand with a preinstalled 5′ phosphate had higher potency than the siRNA with this modification and a 5′-OH (compare **si16** to **si15**). This suggests that the 2′-F/Me modification at position 1 of the antisense strand is tolerated by RISC, but there is some impairment of endogenous phosphorylation. Modification at position 7 of the antisense strand of the siRNA targeting F7 had considerably lower activity than the parent (compare **si17** to **si13**). Potency was, however, increased by modification of position 7 in the siRNA targeting *Ttr* (**si19** to **si20**). In general, single 2′-F/Me-pyrimidine nucleotides in the seed region, modification of the 3′ overhang, and position 1 of the antisense in conjugation with VP were well tolerated, although the effects appear to be sequence-dependent.

Off-Target Effects of siRNAs Modified with 2′-F/Me. Seed-mediated off-target activity contributes to the hepatoxicity of siRNAs in rats, and one way to mitigate this hybridization-based effect is to incorporate thermally destabilizing nucleotides such as GNA in the seed region.[48] To be effective, such thermally destabilizing modifications must maintain on-target activity while reducing off-target activity.[49−56] We measured the effect of 2′-F/Me on off-target activity using a luciferase reporter assay where four tandem seed matches to the siRNA are present in the luciferase 3′-untranslated region (3′UTR).[53,65,66] The siRNAs used in this
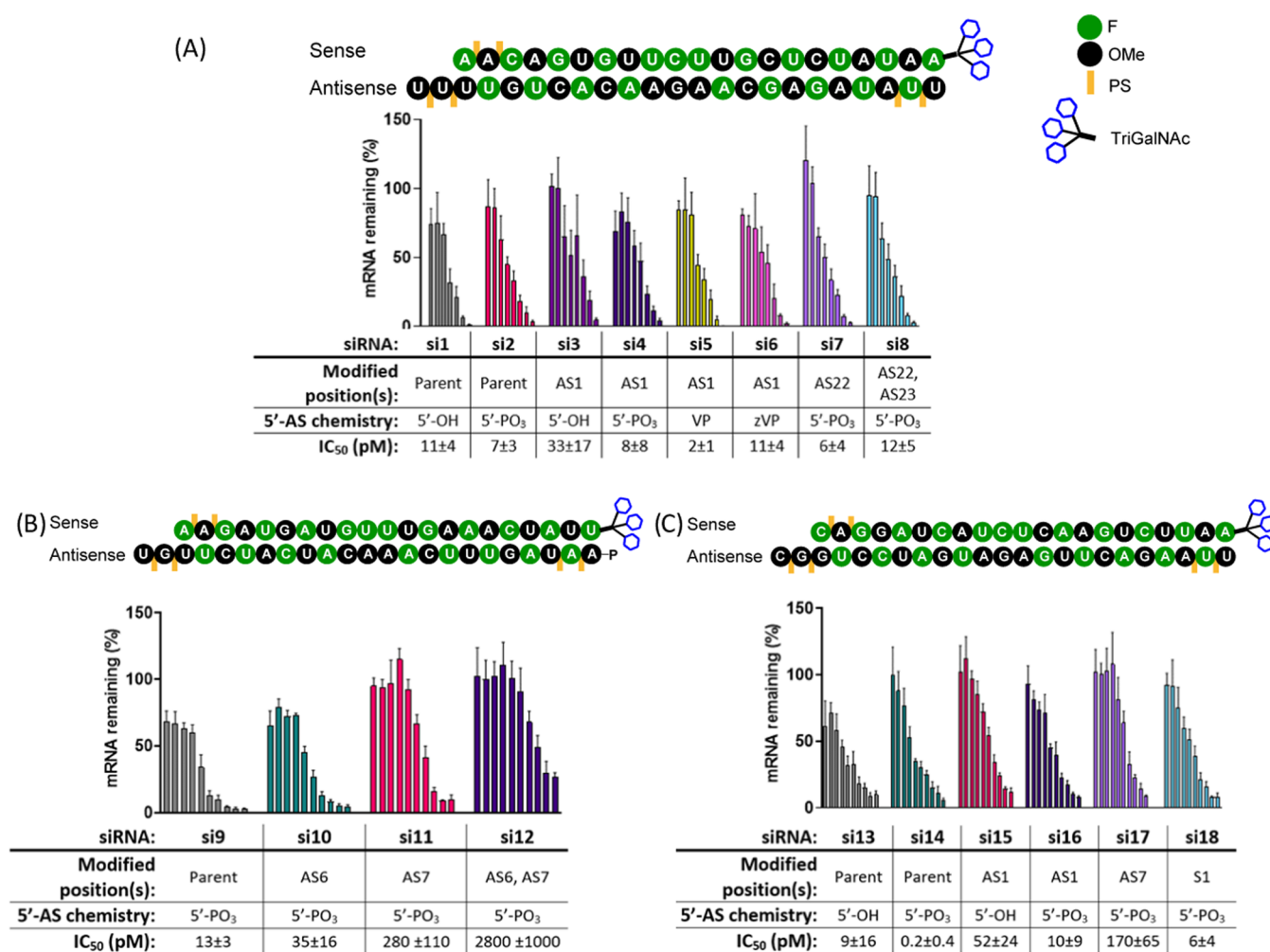
Figure 4. In vitro potencies of fully 2′-modified siRNA targeting (A) *Ttr*, (B) *Pten*, and (C) *F7*. For experimental conditions, see Table 5. The 2′-F and 2′-OMe nucleotides are represented as green or black circles, respectively. A yellow bar represents a PS linkage, VP is 5′-(*E*)-vinyl phosphonate, and zVP is 5′-(*Z*)-vinyl phosphonate. TriGalNAc is triantennary GalNAc. Error bars show standard deviations from the mean.

assay were designed to target *Ttr*: **si19** is the parent, and **si20** is modified with 2′-F/Me at position 7 of the antisense strand. The on-target activity of siRNA with 2′-F/Me in the seed region was similar to the activity of the parent in the luciferase assay for this siRNA sequence. In the assay with endogenous mRNA, the activity of the 2′-F/Me-modified siRNA was approximately two-fold higher (Figure 5). In the reporter assay, the parent siRNA had considerably more off-target activity than **si20** (Figure 5A,B).

To further evaluate the impact of 2′-F/Me on off-target activity, we used RNA sequencing to measure the level of transcriptional dysregulation upon siRNA treatment as previously described.[64] Transfection of the parent siRNA targeting *Ttr* (**si19**) at 50 nM concentration into primary rat hepatocytes resulted in strong up- and downregulation of hundreds of transcripts at 48 h, many of which contained a canonical seed match (Figure 5C). Consistent with the luciferase reporter assay, incorporation of 2′-F/Me at position 7 (**si20**) in the seed region of the antisense strand resulted in considerably less transcriptional dysregulation than observed with the parent siRNA (Figure 5D). These results suggest that the 2′-F/Me modification can mitigate off-target activity in a manner similar to GNA.[68]

In Vivo Activity of 2′-F/Me-Modified siRNA. Encouraged by the in vitro activity of 2′-F/Me-modified siRNAs, we evaluated these siRNAs in mice using two different delivery platforms. First, siRNAs targeting *F7* consisting of a 21-mer RNA duplex with two thymidine overhangs and terminal PS linkages were formulated in LNPs optimized for hepatic delivery.[67] Mice (C57BL/6) were dosed with siRNA at either 0.01 or 0.03 mg/kg, and at 48 h after administration, the serum *F7* levels were quantified. The parent duplex **si21** had an ED$_{80}$, the dose that reduces target protein by 80%, of 3 mg/kg as did the siRNA with a single 2′-F/Me modification at position 2 of the antisense strand (**si22**). The siRNAs with multiple 2′-F/Me modifications (**si23**, **si24**, and **si25**) had dramatically reduced potencies compared to the parent (Figure 6A). These data confirm our in vitro observations that the effects of a single modification are position-dependent and that multiple modifications are not tolerated.

To further assess the positional dependence, we analyzed *F7*-targeting siRNAs conjugated to GalNAc, which can be administered subcutaneously. These siRNAs are 21:23-mer asymmetric duplexes comprising of 2′-OMe and 2′-F nucleotides with terminal PS linkages and a 3′-conjugated GalNAc ligand on the sense strand.[20] siRNAs with 2′-F/Me nucleotides at various positions were evaluated in mice (Figure
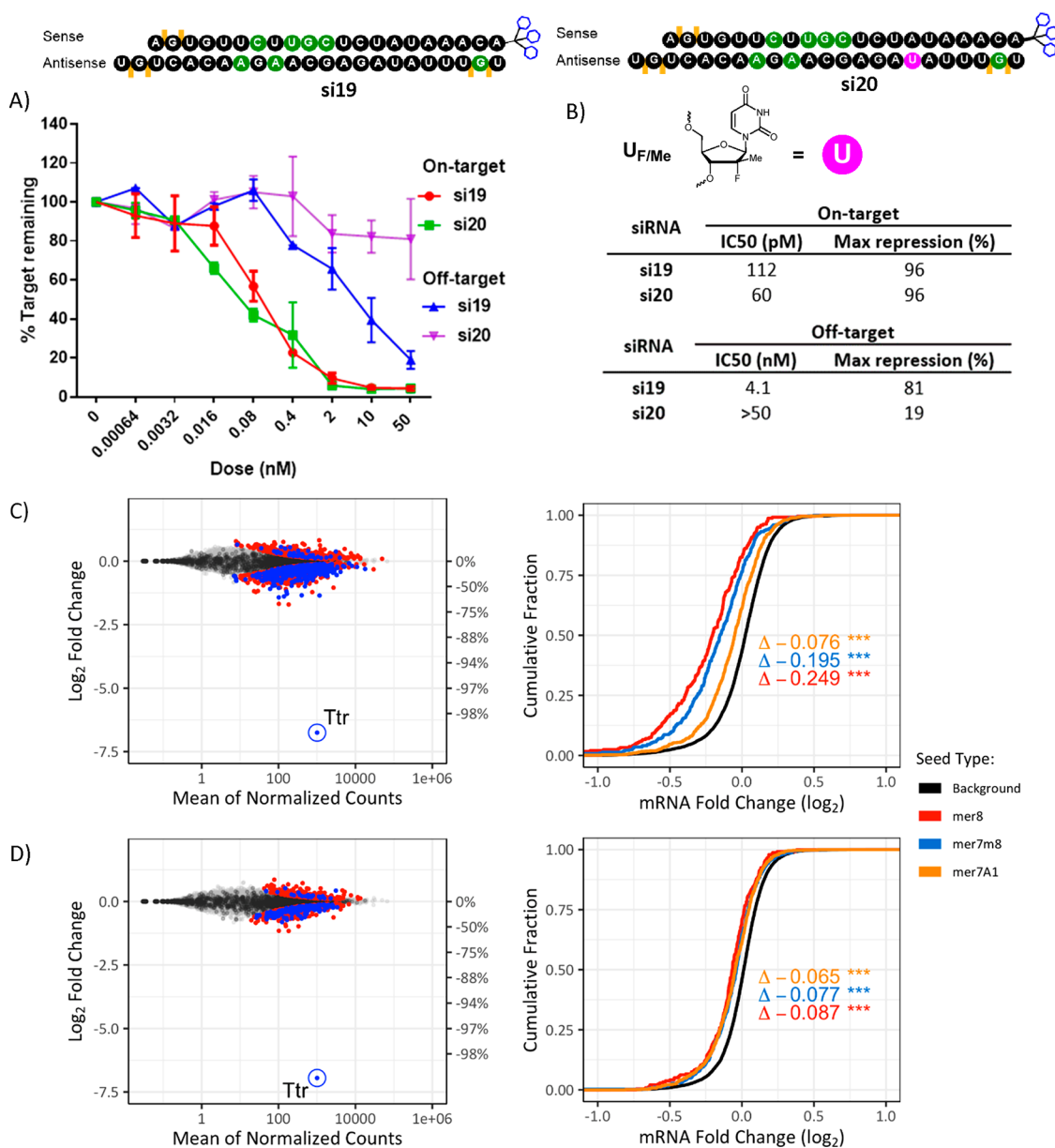
Figure 5. Seed-mediated off-target activity is mitigated by the incorporation of 2′-F/Me at position 7 of the antisense strand. (A) On- and off-target effects were evaluated in a dual-luciferase reporter assay. Luciferase reporter plasmids were cotransfected with indicated siRNAs into COS-7 cells. The cells were harvested for 48 h, and luciferase activity was assayed. Percent target remaining was calculated by dividing the ratio of *Renilla* to firefly luciferase signal at each siRNA concentration by the ratio in the absence of siRNA. (B) On- and off-target IC_{50} and maximum repression values were calculated based on the luciferase assay data. (C and D) Effects of 50 nM of (C) parent siRNA (**si19**) and (D) modified siRNA (**si20**) on on- and off-target gene expression in primary rat hepatocytes. At 48 h after transfection, total RNA was isolated and RNA-seq analysis was performed using standard bioinformatics tools.[61−63] Left: MA plots of $\log_2$ fold change (siRNA treatment/mock-transfection control) vs abundance (average counts) of individual genes. Black [S] and gray [NS] dots represent genes not differentially expressed after siRNA treatment relative to the control. Blue [S] and red [NS] dots represent differentially expressed genes (false discovery rate < 0.05). [S: with a canonical seed match (8mer, 7mer-A1, 7mer-m8)[64] in the gene 3′UTR, NS: without a 3′UTR seed match]. On-target knockdown of *Ttr* is indicated by the circled dot. Right: Cumulative distribution plots, which visualize the fraction of genes below a given $\log_2$ fold change, show the magnitude of dysregulation for gene sets in different canonical 3′UTR seed match categories relative to the background (black, NS) for the parent siRNA **si19** in panel (C) vs the modified siRNA **si20** in panel (D).

6B). Treatment with the parent siRNA (**si26**) at a dose of 1 mg/kg resulted in a 60% reduction in circulating F7 protein, when assayed 10 days after administration. The siRNA with a 2′-F/Me at position 20 of the antisense strand (**si27**) had activity similar to that of the parent. However, when two 2′-F/Me nucleotides were incorporated at positions 18 and 20 of the antisense strand (**si28**), there was only a 40% reduction in F7 when dosed at 3 mg/kg, and the siRNA with three 2′-F/Me

modifications in the antisense strand was even less potent (**si29**). Multiple 2′-F/Me modifications were not well tolerated on the sense strand; **si30** with three modifications at positions 9−11 had lower activity compared to the parent. The optimal activity requires sense strand cleavage in this region,[43,45,47] and this cleavage is likely inhibited by the consecutive placement of 2′-F/Me in these positions due to the increased resistance to nuclease-mediated degradation.
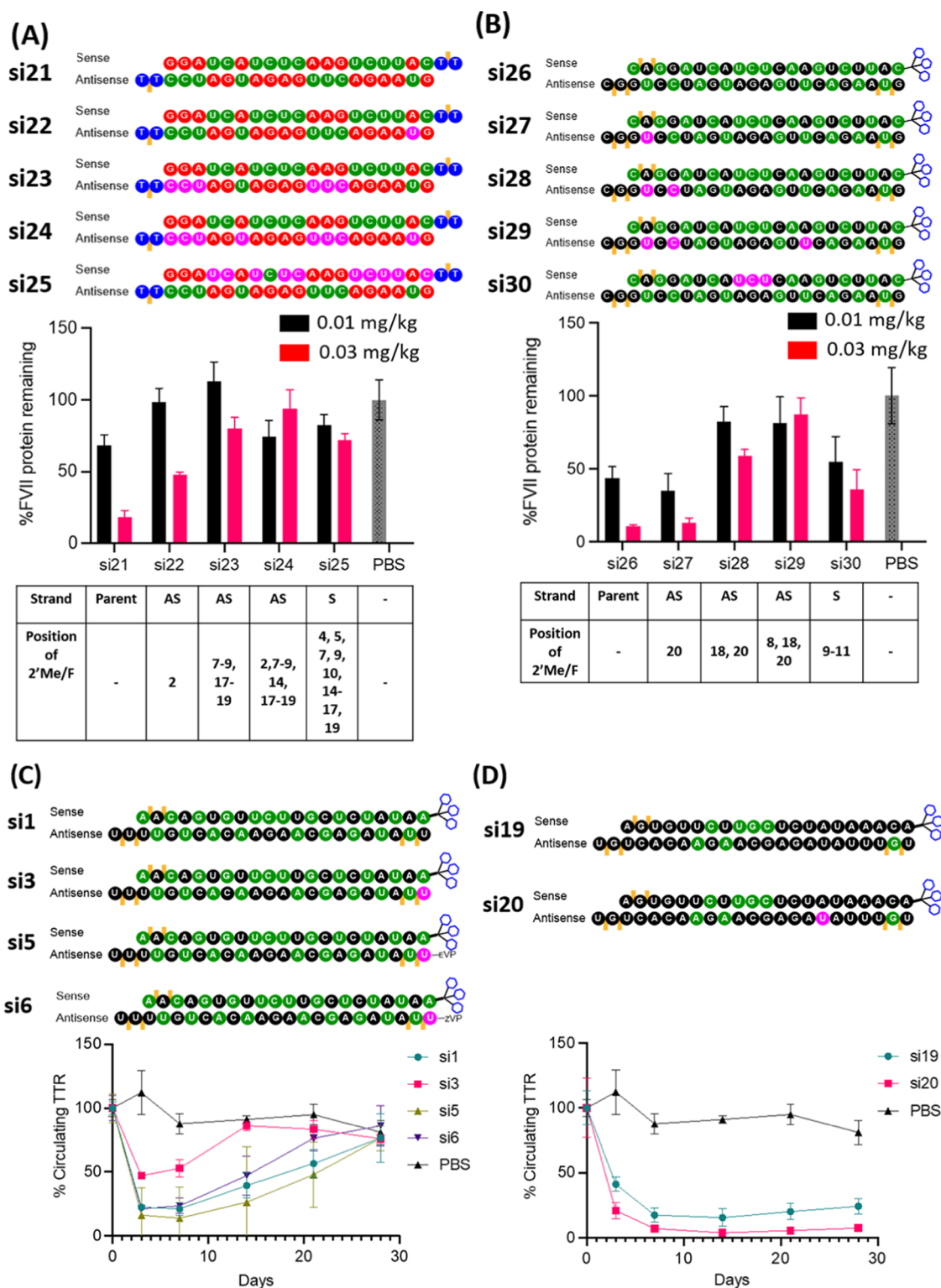
Figure 6. Impact of 2′-F/Me modifications on in vivo activity. (A and B) C57BL/6 mice (*n* = 3) received a single dose of either 1 mg/kg (black) or 3 mg/kg (pink) of (A) *F7*-targeted siRNA (**si21**, **si22**, **si23**, **si24**, or **si25**) as an LNP formulation intravenously or (B) *F7*-targeted GalNAc-conjugated siRNA (**si26**, **si27**, **si28**, **si29**, or **si30**) subcutaneously. Control animals received PBS (gray). Serum F7 protein levels were measured at parent nadir: 48 h for LNP formulations and 10 days for GalNAc conjugates. (C and D) C57BL/6 mice (*n* = 3) received a single dose of 1 mg/kg of *Ttr*-targeting siRNA with (C) terminal 2′-F/Me modifications (**si1**, **si3**, **si5**, or **si6**) or (D) internal 2′-F/Me modifications (**si19** or **si20**), and serum protein levels were monitored until day 28. In ball diagrams of oligonucleotides, 2′-F, 2′-OMe, 2′-F/Me, deoxyribonucleotides, and ribonucleotides are represented as green, black, blue, pink, and red circles, respectively. A yellow bar represents a PS linkage. Data points were normalized to predose F7 or TTR levels, and values are group means ± standard deviation (SD).

To further understand the impact of modifying position 1 of the antisense strand, which interacts with the MID domain of

Ago2 after 5′ phosphorylation in the cell, in vivo potency of *Ttr*-targeted siRNAs modified at this position was assessed in

Journal of the American Chemical Society
pubs.acs.org/JACS
Article
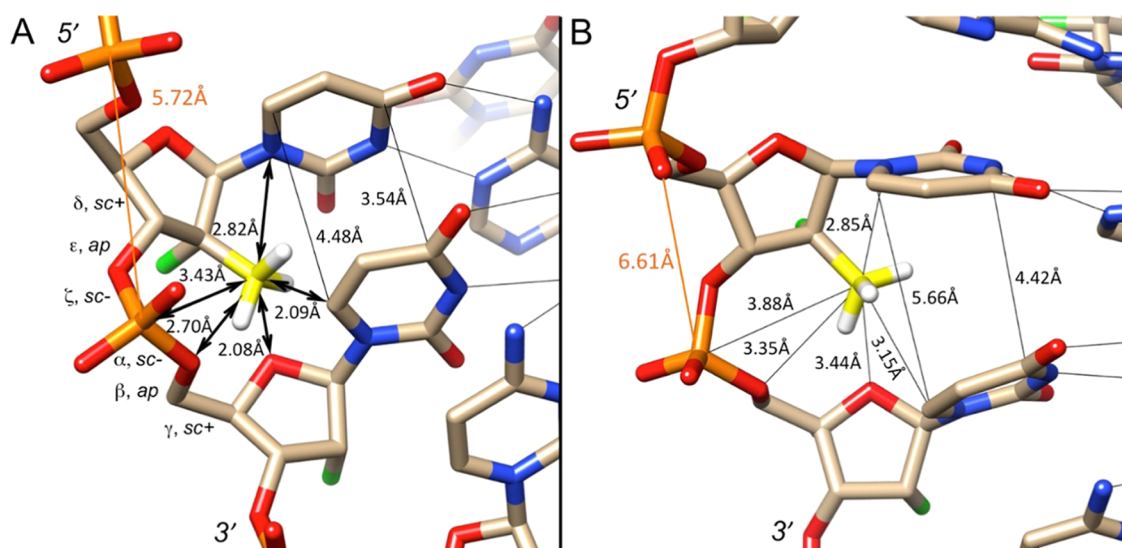
Figure 7. (A) Model illustrating steric clashes as a consequence of the introduction of a 2′-β-C-methyl group on a single nucleotide in a 2′-F-modified RNA A-form duplex (PDB ID 3P4A).[72] (B) Relaxed model after molecular mechanics minimization. This structure lacks clashes between the methyl group and its nearest neighbors, but stacking is lost between uridines. Methyl carbon and hydrogen atoms are colored in yellow and white, respectively, and fluorine atoms are light green. Short contacts are indicated with arrows. Watson−Crick hydrogen bonds and additional selected distances are shown with thin solid lines, and backbone torsion angle ranges are depicted on the left in panel (A).
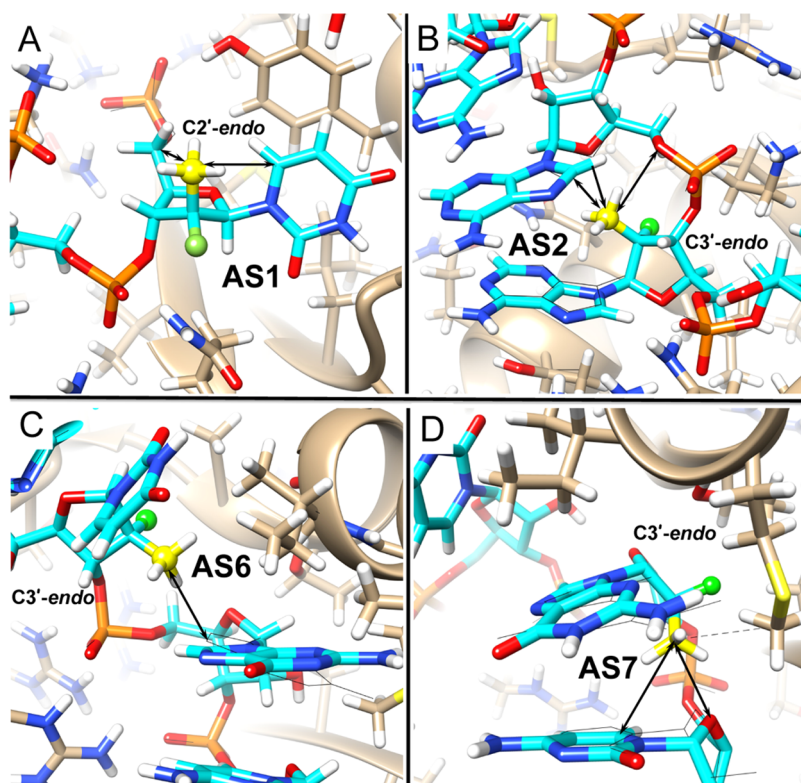
Figure 8. Modeled conformations of 2′-F/Me nucleotides at positions (A) 1, (B) 2, (C) 6, and (D) 7 of the antisense strand incorporated into the siRNA antisense strand bound to human Ago2. Methyl carbon and hydrogen atoms are colored in yellow and white, respectively, and fluorine atoms are light green. Short contacts are indicated with arrows. The initial conformation of the antisense strand as seen in the crystal structure of the human Ago2:miR−20a complex (PDB ID 4F3T)[60] is shown with thin black lines. A potentially favorable contact is indicated by a dashed line in panel (D).

mice up to day 28 after 1 mg/kg subcutaneous administration (Figure 6C). As expected, the siRNA with 2′-F/Me at position 1 (**si3**) was less active than the parent, possibly because it does not serve as a kinase substrate. In support of this hypothesis, the siRNA with (E)-VP (**si5**) had slightly improved potency

relative to the parent **si1**. (Z)-VP (**si6**) had slightly reduced activity. Thus, a 5′-modification with (E)-VP and 2′-F/Me at position 1 of the antisense siRNA in combination with other optimized modifications results in an siRNA with in vivo efficacy comparable to (or slightly better than) the parent
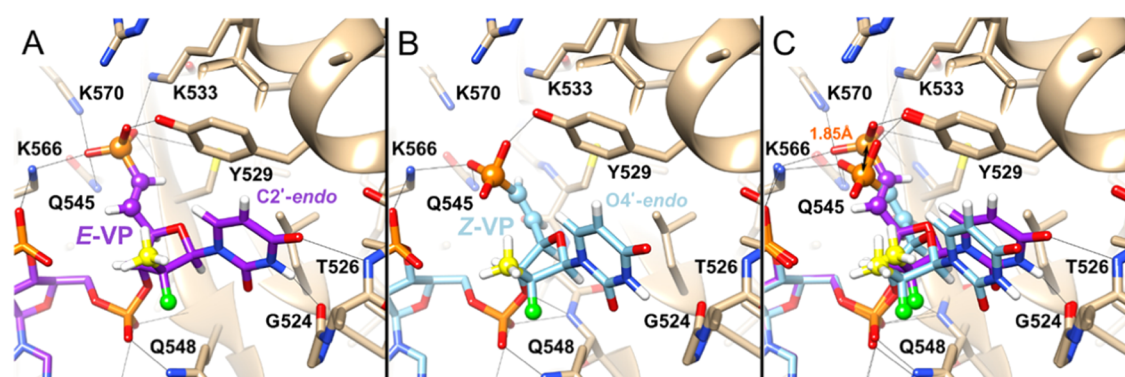
Figure 9. Models of RNA strands with VP-2′-F/Me-modified nucleotides at position 1 bound to the human Ago2 MID domain. (A) Model with (*E*)-VP with the C2′-*endo* sugar conformation; carbon atoms colored in purple. (B) Model with (*Z*)-VP with the O4′-*endo* sugar conformation; carbon atoms colored in light blue. (C) Overlay of the (*E*)-VP and (*Z*)-VP nucleotide regions. The distance between the two phosphorus atoms (1.85 Å) is indicated with a double arrow. VP moieties, 2′-F (light green) and 2′-Me carbon (yellow) of 2′-F/Me are highlighted in ball-and-stick mode, salt bridges and hydrogen bonds are drawn with thin solid lines, and selected Ago2 side chains are labeled.

(**si1**). Interestingly, the siRNA modified with both 2′-F/Me and (*Z*)-VP (**si6**) had silencing activity only slightly less than the parent (**si1**). This is the first observation of the in vivo silencing activity of a (*Z*)-VP-modified siRNA.[41−47] This suggests that the steric impact of 2′-F/Me at position 1 may result in a more favorable conformation than when the (*Z*)-VP is used in conjunction with a 2′-OMe or a 2′-F substituent.

Next, we compared the in vivo activity of a *Ttr*-targeted siRNA, **si19**, which has off-target effects as demonstrated by previous transcriptome analyses,[48,68] to that of the siRNA modified at position 7 in the seed region of the antisense strand with 2′-F/Me (**si20**). The pharmacodynamic profile of the 2′-F/Me-modified siRNA indicated that efficacy was improved relative to the parent siRNA (Figure 6D). Thus, modification with 2′-F/Me may be a promising approach for improving the therapeutic index of siRNAs as this modification in the seed region can mitigate off-target gene silencing as shown in cell-based assays without adversely impacting potency.

Structural Consequences of 2′-F/Me in siRNA. Crystal structures of β-D-2′-deoxy-2′-α-fluoro-2′-β-C-methyl-cytidine[69] and the corresponding uridine nucleotide prodrug PSI-7977[70] revealed that the modified sugar adopts a C3′-*endo* pucker. In an A-form RNA oligonucleotide with standard *sc*-/*ap*/*sc*+/*sc*+/*ap*/*sc*- backbone torsion angles (α to ζ) and riboses in the C3′-*endo* conformation, the pseudoequatorial orientation of the 2′-β-C-methyl group results in short contacts to base, sugar, and phosphate atoms of the 3′-adjacent nucleotide (Figure 7A). Some of these barely exceed the van der Waals radius of a methyl group (2 Å), which likely explains the observed destabilizations of RNA duplexes with 2′-F/Me U or C on one strand (Table 1). Avoiding these short contacts requires conformational changes that probably entail adjustments in the backbone and glycosidic torsion angles that result in local base unstacking. Indeed, energy minimization of the model duplex containing a 2′-F/Me residue using a standard molecular mechanics approach (Amber 14ff, UCSF Chimera)[71] resulted in close distances between the methyl group and atoms from the 3′-adjacent nucleotide. Avoiding these internucleotide steric conflicts resulted in a loss of stacking between the uracil bases (Figure 7B). Further, these changes were accompanied by a stretching of the sugar-phosphate backbone, manifested in an increased intrastrand phosphate-phosphate distance from 5.7 Å in the native duplex

to 6.6 Å in the duplex with a modified residue (Figure 7B). The altered spacing between phosphates and associated differences in the local electrostatic surface potential probably contribute to the improved resistance to nuclease degradation afforded by 2′-F/Me relative to 2′-F nucleotides (Tables 3 and 4).

To gain a better understanding of the structural origins of the observed activities of siRNAs with 2′-F/Me nucleotides incorporated at position 1, 2, or 6 in the antisense strand, we turned to the crystal structure of human Ago2 in complex with miR-20a (PDB ID 4F3T).[60] The modified nucleotide is tolerated quite well at positions 1 and 6 but results in a marked loss in activity at position 2 (Figure 4). At the 5′-terminal position of the antisense strand, the phosphate group and base are held tightly in place by multiple interactions including salt bridges involving the phosphate group (Figure 8A). The ribose of the nucleotide at position 1 of the antisense strand adopts a C2′-*endo* B-DNA-like pucker, the antisense strand makes a sharp turn between positions 1 and 2, and the tight grip of the protein continues at positions 2 and 3. We used UCSF Chimera to add the methyl group in the 2′-β-C orientation to sugars at positions 1, 2, 6, and 7 and replaced the native 2′-hydroxyl group with fluorine. The modified complex was then relaxed using molecular mechanics (Amber 14ff) as implemented in UCSF Chimera.[71] Because of multiple interactions between protein and each nucleotide in the complex, the computational approach used does not result in significant movements of atoms triggered by short contacts arising from the additional methyl group.

At position 1, the pseudoaxial orientation of the 2′-β-C-methyl group leads to two relatively tight intranucleoside 1···5 contacts to C5′ and N1 (3.5 and 3.1 Å, respectively) in the refined model (Figure 8A). Unless the sugar is flipped into a different pucker, these are difficult to avoid. However, the mold provided by Ago2 likely precludes substantial conformational changes. There are no other conflicts as a consequence of the additional methyl group, and we conclude that a 2′-F/Me-modified nucleotide at position 1 of the antisense strand is quite well accommodated by the Ago2 binding site, consistent with the high activity of siRNA with this modification (Figure 4). Conversely, the incorporation of a modified nucleotide at position 2 results in clashes between the methyl group and atoms of the base, sugar, and phosphate moieties from the 3′-adjacent nucleotide (Figure 8B). Expansion of the sugar-

phosphate backbone between positions 2 and 3 interferes with binding by Ago2, thus providing a structural rationalization for why the 2′-F/Me nucleotide is poorly tolerated at position 2 of the antisense strand. Finally, a strong kink between positions 6 and 7, as seen in the crystal structure of the Ago2 complex,[60] provides generous space for the accommodation of a 2′-F/Me-modified nucleotide at position 6. A somewhat short contact in the initially built model between the methyl group and the C8-H position of the guanidine at position 7 is mitigated by a slight rotation of the base around the glycosidic bond with a concomitant increase of the Me⋯C8 distance to approximately 3.4 Å in the refined model (Figure 8C). The computational model thus makes clear why the 2′-F/Me nucleotide at position 6 does not impair RNAi activity. The 2′-F/Me nucleotide incorporated at position 7 also resulted in a somewhat tight spacing between the 2′-methyl group and C6 of the base of the 3′-adjacent nucleotide (Figure 8D). In the refined model, the distance is 3.5 Å as the two bases are slightly pushed apart. However, a close contact between the 2′-methyl and the 4′-oxygen of position 8 remains (2.8 Å). This clash is not seen between the corresponding atoms of positions 6 and 7 due to the kink between these residues (Figure 8C). An interesting consequence of the modification at position 7 is a potentially favorable contact (3.6 Å) between the 2′-methyl moiety and the methyl group of the side chain of Met-364 of Ago2 (Figure 8D).

To model the interactions of (E)-VP and (Z)-VP 2′-F/Me uridines at position 1 of the antisense strand, we started from the crystal structure of human Ago2 in complex with miR-20a.[24] In this structure, the (E)-VP has an unusual C2′-endo (South) sugar pucker with a pseudoaxial 2′-β-C-Me substituent (Figure 9A). In the crystal structure with 5′-phosphorylated miRNA, the P-O5′-C5′-C4′ torsion angle is nearly anti-periplanar (ap) and the (E)-VP moiety is therefore accommodated with virtually no change in the orientation of the phosphate relative to the parent structure. The (Z)-VP model features an O4′-endo (East) sugar pucker, and neither the 2′-F nor the 2′-Me substituent is in a pseudoaxial orientation (Figure 9B). The phosphate engages in a salt bridge with Lys-566 and forms hydrogen bonds to Tyr-529 and Gln-545, and an overlay of the (E)-VP and (Z)-VP models shows that the phosphates are only 1.85 Å apart (Figure 9C). The (Z)-VP phosphate does not reach quite as deep into the binding pocket as does the phosphate of the (E)-VP moiety; however, the (Z)-VP phosphate is able to establish favorable electrostatic interactions. A further slight change between the (E)-VP and (Z)-VP models concerns the orientation of the uracil base vis-à-vis the Tyr-529 side chain: In the (Z)-VP model, the base is partially unstacked with a vertical shift of approximately 1 Å relative to the (E)-VP uracil ring (Figure 9C). Overall, the model of the (Z)-VP 2′-F/Me uridine-modified strand is consistent with the observed in vivo potency of this modification (Figure 6), which is in contrast with the poor activity of the Z isomer of VP in the context of 2′-OMe or 2′-F chemistries.[41−47]

The molecular reasons for protection against the attack by exonucleases afforded by the 2′-F/Me modification (Figures 2 and 3) were assessed using models of complexes based on the crystal structures of *Drosophila melanogaster* 5′-3′ exoribonuclease Xrn1 bound to a 5′-phosphorylated trinucleotide P-d(TTT) (PDB ID 2Y35)[73] and *Escherichia coli* DNA polymerase I Klenow fragment 3′−5′-exonuclease bound to a DNA tetramer with a single Sp-PS moiety 3′-d(T$_{PS}$TTT)-5′

(PDB ID 1KSP).[74] In both cases, terminal and penultimate dT were replaced by 2′-F/Me-U. The sugar puckers in the parent crystal structures were not altered: Sugars adopt a C2′-endo conformation at the Xrn1 active site (Figure 10A) and a C3′-
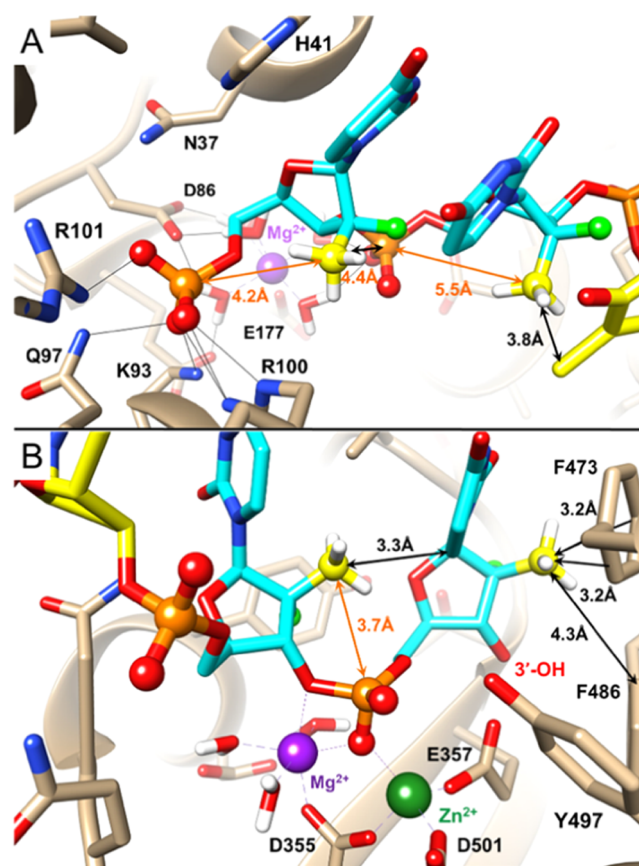
Figure 10. Origins of the improved resistance to exonuclease degradation by 2′-F/Me-modified oligonucleotides. (A) Model of oligo(dT) (yellow carbons) with two 5′-terminal 2′-F/Me-U residues (cyan carbons) bound to the active site of *D. melanogaster* Xrn1 5′-exoribonuclease. (B) Model of oligo(dT) (yellow carbons) with two 3′-terminal 2′-F/Me-U residues (cyan carbons) bound to the active site of *E. coli* DNA polymerase I Klenow fragment 3′-exonuclease. Distances between the 2′-Me carbon and phosphorus atoms are indicated with orange arrows. Distances between the 2′-Me carbon and selected protein and DNA atoms are indicated with black arrows. 2′-F (light green), 2′-Me carbon (yellow), phosphorus (orange), nonbridging phosphate oxygens (red), and metal ions (green) are highlighted in ball-and-stick mode. Salt bridges and hydrogen bonds are drawn with thin solid lines, metal ion coordination spheres are drawn with dashed lines, and selected Xrna1 and Klenow fragment side chains are labeled. All water molecules except those coordinated to catalytic metal ions were omitted.

endo conformation at the active site of DNA polymerase I Klenow exonuclease (Figure 10B). In the active site of Xrn1, the methyl group of the 5′-terminal 2′-F/Me-U sits quite close to the 5′ phosphate and the first bridging phosphate (4.2 and 4.4 Å, respectively, below the sum of the van der Waals radii, 4.8 Å). The methyl group of the 3′-terminal 2′-F/Me-U at the active site of Klenow 3′-exonuclease points into a tight space limited by two Phe residues that form the floor of the active site (the closest distance is 3.2 Å; below the sum of the van der Waals radii, 3.5 Å). These analyses help rationalize the better protection of the 2′-F/Me modification relative to 2′-F alone.
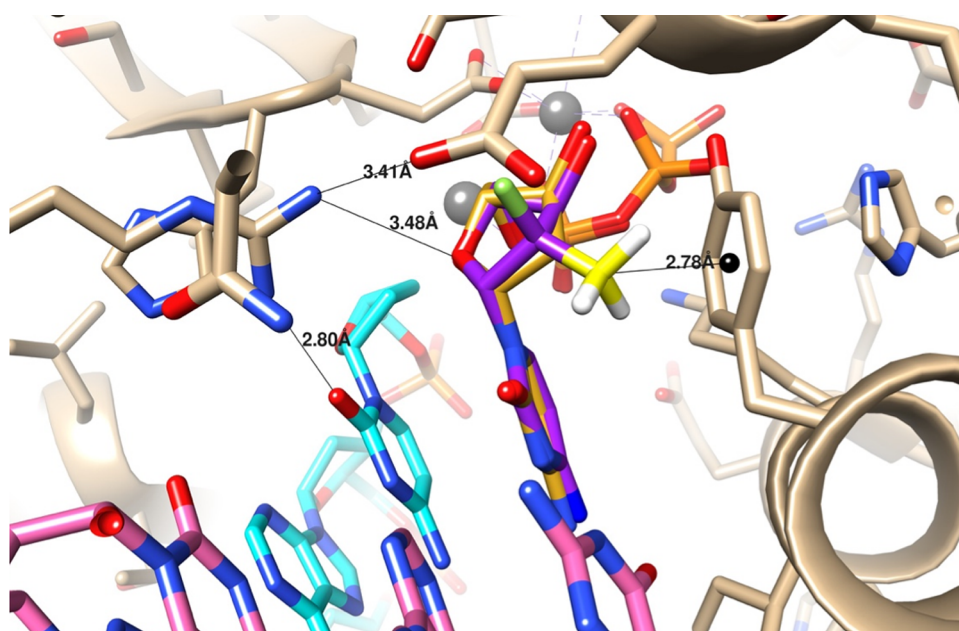
Figure 11. Origin of the inability of POLG to incorporate a 2′-F/Me-modified nucleotide. The active site in the crystal structure of a ternary POLG•DNA•dCTP Mg^{2+} complex (PDB ID 4ZTZ) is shown. The view is into the minor groove of the duplex formed by the DNA template (pink carbon atoms) and primer (cyan carbon atoms) strands. The 2′-F/Me CMP (purple carbon atoms) is superimposed on the incoming dCTP (gold carbon atoms). Two Mg^{2+} ions are visible in the background as gray spheres. The distance of 2.78 Å between the 2′-F/Me methyl carbon (highlighted in yellow) and the center of mass of the Tyr-951 ring (black dot) is consistent with a short contact (the sum of the van der Waals radii for the methyl group, 2 Å, and phenyl carbons, 1.5 Å, is 3.5 Å). Selected distances are shown with thin solid lines.

Structural Rationalization for Poor Incorporation of 2′F/Me Nucleotides by Mitochondrial Polymerase Gamma. Native NTPs (rCTP, rUTP, dCTP, and dTTP) are efficiently incorporated by the mitochondrial DNA and RNA polymerases POLG and POLRMT, respectively.[40,75] Although 2′-F monomers are incorporated at high concentrations by POLRMT, the 2′-F/Me-modified nucleotide analogues are not substrates for either mitochondrial polymerase.[15−17] The inability of POLG to incorporate 2′-F/Me-modified residues can be readily explained by an unfavorable interaction between the 2′-Me moiety and the "gatekeeper" residue Tyr-951 at the active site. When a 2′-F/Me CMP from a refined duplex structure (C3′-endo pucker) is superimposed on the incoming dCTP in the crystal structure of the ternary POLG complex[76] (PDB ID 4ZTZ), the gem-hetero-substituted methyl group points directly into the ring of that tyrosine thereby creating a clash (Figure 11).

CONCLUSIONS

Sofosbuvir is a 2′-F/Me ribonucleotide prodrug that has proven to be of immense value in the treatment of HCV infection. Its 5′-phosphorylated form effectively inhibits the viral RNA polymerase, and it has an excellent safety profile. Inspired by the pharmacology of this drug, we evaluated this core 2′-gem-hetero-substituted C3′-endo nucleoside backbone in oligonucleotide-based RNAi therapeutics. We demonstrated a facile synthesis of 2′-F/Me phosphoramidites and the corresponding uridine (E)-VP and (Z)-VP phosphoramidites. Contrary to the expectation that the C3′-endo sugar pucker of the 2′-F/Me ribonucleotide would stabilize complementary RNA binding, 2′-F/Me modifications were thermally destabilizing in both RNA:RNA and RNA:DNA duplexes and appeared to perturb the duplex geometry on the 3′ side of the modification. We speculate that this perturbation results in

the enhanced stabilization toward 5′- and 3′-exonuclease-mediated degradation provided by terminal 2′-F/Me modification. Steric conflicts due to the 2′-β-C-methyl group likely account for the destabilization of interactions with complementary oligonucleotides and protection against degradation by nucleases.

Analyses of siRNAs modified with 2′-F/Me revealed the positional dependence of RNAi activity in both cell culture and mice. When siRNAs were modified with several 2′-F/Me residues or when only position 2 of the antisense strand was modified, potency was considerably lower than that of parent siRNAs when delivered into cells as either an LNP formulation or a GalNAc conjugate. The loss of activity due to substitution at position 2 is not surprising as only 2′-H, 2′-OH, and 2′-F are tolerated at this position; even 2′-OMe impairs silencing.[21] Substitution with 2′-F/Me caused a kink in the antisense strand as shown by molecular modeling, so we speculate that multiple 2′-F/Me substitutions weaken interactions with Ago2 and result in less stable duplex formation with target mRNA, explaining the loss of potency due to multiple substitutions. Interestingly, the 2′-F/Me modification was well tolerated at position 1 of the antisense strand in conjunction with either the (E)-5′-VP or the (Z)-VP isomer. This was interesting because (E)-VP is tolerated but (Z)-VP is not when position 1 of the antisense strand is a natural ribonucleotide, a 2′-F, or a 2′-OMe-modified residue. When position 1 of the antisense strand is 2′-F/Me, the (Z)-VP phosphate appears to establish favorable electrostatic interactions due to the distortion provided by the 2′-β-C-methyl group.

The 2′-F/Me modification in the seed region, at position 6 or 7, was well tolerated in two of the three tested siRNAs. Importantly, in cell-based assays, 2′-F/Me nucleotides at these positions mitigated off-target effects in a manner similar to other thermodynamically destabilizing modifications like

GNA.[48] A 2′-F/Me nucleotide may mitigate off-target effects both by conformational preorganization of the antisense strand and by thermodynamic destabilization of the duplex between the antisense strand of the siRNA and target mRNA. The preorganization is driven by the methyl group, which forces the strand to kink, thus facilitating the loading of the guide strand into Ago2. Further, the kink between positions 6 and 7, as seen in the crystal structure of the Ago2 complex,[60] provides generous space for the accommodation of a 2′-F/Me-modified nucleotide at position 6 or 7. The thermodynamic destabilization due to 2′-F/Me nucleotides is expected to result in reduced incorporation of mRNAs with mismatches opposite the guide strand. Even in the crystal structure of Ago2 with a duplex bound (PDB ID 4W5T),[77] a considerable roll-bend of approximately 20 degrees between guide strand nucleobases at positions 6 and 7 persists. That the degree of kinking is reduced in the case of the Ago2 complex with the duplex of the antisense strand and mRNA target compared to the complex with the miR-20a single strand does not come as a surprise. The enzyme must be able to sculpt the RNA single strand relative to the more rigid duplex, where it has to pry open stacked base pairs to induce the kink. The steric challenges posed by a 2′-F/Me nucleotide are accommodated in either complex, irrespective of the degree of kinking compared to a standard duplex. We hypothesize that conformational preorganization of the antisense strand and thermal destabilization of the duplex between the antisense strand and target mRNA contribute to the reduction in off-target effects seen with both (S)-GNA[48] and 2′-F/Me modifications; however, the underlying mechanism of preorganization is likely different for GNA and 2′-F/Me nucleotides. GNA has a shorter backbone compared to DNA and RNA, which results in tighter intrastrand phosphate-phosphate distances at sites of modifications (ca. 5.5 Å). This is exactly the distance between phosphates seen at the site of the kink in miR-20a bound to Ago2. In the case of the 2′-F/Me modification, the tendency to alter the trajectory of the strand occurs at the level of the nucleobase in that the methyl group pushes away the adjacent base, thereby inducing a roll-bend at that site.

An attractive feature of 2′-F/Me nucleotides is that they are poor substrates for mitochondrial polymerases;[78] thus, 2′-F/Me nucleotides may improve site-specific potency, duration, and safety of siRNAs. Whereas the 2′-F ribonucleoside does not interfere with Ago2 binding or subsequent slicer activity when incorporated at any positions of an siRNA,[79] the present study clearly demonstrated that tolerance for the 2′-F/Me nucleoside in an siRNA is position-dependent. Encouraged by our results, we plan to evaluate this modification systematically at each position of siRNAs targeting various mRNAs. The syntheses of purine 2′-F/Me nucleosides have been previously described,[80−82] but evaluation of these modifications in the context of siRNA will necessitate the synthesis of phosphoramidites and solid supports, which is ongoing. Finally, 2′-F/Me nucleotides in siRNAs that target viral transcripts or transcripts involved in host pathways dysregulated during viral infection may have a dual mechanism as monomer metabolites could act as inhibitors of viral polymerases as well as mediators of RNAi.

■ ASSOCIATED CONTENT

Ⓢ Supporting Information

The Supporting Information is available free of charge at https://pubs.acs.org/doi/10.1021/jacs.2c01679.

Experimental section; MS analysis of oligonucleotides; additional thermal denaturation data; exonuclease degradation plots; in vitro IC_{50} curves; and ^{1}H, ^{13}C, and 2D NMR spectra for all characterized compounds (PDF)

■ AUTHOR INFORMATION

Corresponding Author

Muthiah Manoharan − *Alnylam Pharmaceuticals, Cambridge, Massachusetts 02142, United States;* ⦿ orcid.org/0000-0002-7931-1172; Email: mmanoharan@alnylam.com

Authors

Dale C. Guenther − *Alnylam Pharmaceuticals, Cambridge, Massachusetts 02142, United States*

Shohei Mori − *Alnylam Pharmaceuticals, Cambridge, Massachusetts 02142, United States;* ⦿ orcid.org/0000-0001-8472-8055

Shigeo Matsuda − *Alnylam Pharmaceuticals, Cambridge, Massachusetts 02142, United States*

Jason A. Gilbert − *Alnylam Pharmaceuticals, Cambridge, Massachusetts 02142, United States*

Jennifer L. S. Willoughby − *Alnylam Pharmaceuticals, Cambridge, Massachusetts 02142, United States*

Sarah Hyde − *Alnylam Pharmaceuticals, Cambridge, Massachusetts 02142, United States*

Anna Bisbe − *Alnylam Pharmaceuticals, Cambridge, Massachusetts 02142, United States*

Yongfeng Jiang − *Alnylam Pharmaceuticals, Cambridge, Massachusetts 02142, United States*

Saket Agarwal − *Alnylam Pharmaceuticals, Cambridge, Massachusetts 02142, United States*

Mimouna Madaoui − *Alnylam Pharmaceuticals, Cambridge, Massachusetts 02142, United States*

Maja M. Janas − *Alnylam Pharmaceuticals, Cambridge, Massachusetts 02142, United States*

Klaus Charisse − *Alnylam Pharmaceuticals, Cambridge, Massachusetts 02142, United States*

Martin A. Maier − *Alnylam Pharmaceuticals, Cambridge, Massachusetts 02142, United States*

Martin Egli − *Department of Biochemistry, School of Medicine, Vanderbilt University, Nashville, Tennessee 37232, United States;* ⦿ orcid.org/0000-0003-4145-356X

Complete contact information is available at:
https://pubs.acs.org/10.1021/jacs.2c01679

Notes

The authors declare no competing financial interest.

■ DEDICATION

This publication is dedicated to the loving memories of Professors A. R. Venkitaraman, Divakar Masilamani, P. T. Chellappa, Cooksley B. Jawahar Singh, and K. Jayaraj, Professors of Chemistry at the American College, Madurai, Tamil Nadu, India, for their several decades of inspiring teaching, dedicated service, and guidance and for seeding interest in chemistry and chemical research in their students.

■ REFERENCES

(1) Elbashir, S. M.; Harborth, J.; Lendeckel, W.; Yalcin, A.; Weber, K.; Tuschl, T. Duplexes of 21-nucleotide RNAs mediate RNA interference in cultured mammalian cells. *Nature* **2001**, *411*, 494−498.

(2) Wang, H. W.; Noland, C.; Siridechadilok, B.; Taylor, D. W.; Ma, E.; Felderer, K.; Doudna, J. A.; Nogales, E. Structural insights into RNA processing by the human RISC-loading complex. *Nat. Struct. Mol. Biol.* **2009**, *16*, 1148−1153.

(3) Meister, G.; Landthaler, M.; Patkaniowska, A.; Dorsett, Y.; Teng, G.; Tuschl, T. Human Argonaute2 mediates RNA cleavage targeted by miRNAs and siRNAs. *Mol. Cell* **2004**, *15*, 185−197.

(4) Liu, J.; Carmell, M. A.; Rivas, F. V.; Marsden, C. G.; Thomson, J. M.; Song, J. J.; Hammond, S. M.; Joshua-Tor, L.; Hannon, G. J. Argonaute2 is the catalytic engine of mammalian RNAi. *Science* **2004**, *305*, 1437−1441.

(5) Hammond, S. M.; Aartsma-Rus, A.; Alves, S.; Borgos, S. E.; Buijsen, R. A. M.; Collin, R. W. J.; Covello, G.; Denti, M. A.; Desviat, L. R.; Echevarría, L.; Foged, C.; Gaina, G.; Garanto, A.; Goyenvalle, A. T.; Guzowska, M.; Holodnuka, I.; Jones, D. R.; Krause, S.; Lehto, T.; Montolio, M.; Van Roon-Mom, W.; Arechavala-Gomeza, V. Delivery of oligonucleotide-based therapeutics: challenges and opportunities. *EMBO Mol. Med.* **2021**, *13*, No. e13243.

(6) Xiong, H.; Veedu, R. N.; Diermeier, S. D. Recent Advances in Oligonucleotide Therapeutics in Oncology. *Int. J. Mol. Sci.* **2021**, *22*, 3295.

(7) Smith, C. I. E.; Zain, R. Therapeutic Oligonucleotides: State of the Art. *Annu. Rev. Pharmacol. Toxicol.* **2019**, *59*, 605−630.

(8) Shen, X.; Corey, D. R. Chemistry, mechanism and clinical status of antisense oligonucleotides and duplex RNAs. *Nucleic Acids Res.* **2018**, *46*, 1584−1600.

(9) Stein, C. A.; Castanotto, D. FDA-Approved Oligonucleotide Therapies in 2017. *Mol. Ther.* **2017**, *25*, 1069−1075.

(10) Crooke, S. T.; Witztum, J. L.; Bennett, C. F.; Baker, B. F. RNA-Targeted Therapeutics. *Cell Metab.* **2018**, *27*, 714−739.

(11) Setten, R. L.; Rossi, J. J.; Han, S.-p. The current state and future directions of RNAi-based therapeutics. *Nat. Rev. Drug Discovery* **2019**, *18*, 421−446.

(12) Roberts, T. C.; Langer, R.; Wood, M. J. A. Advances in oligonucleotide drug delivery. *Nat. Rev. Drug Discovery* **2020**, *19*, 673−694.

(13) Akinc, A.; Maier, M. A.; Manoharan, M.; Fitzgerald, K.; Jayaraman, M.; Barros, S.; Ansell, S.; Du, X.; Hope, M. J.; Madden, T. D.; Mui, B. L.; Semple, S. C.; Tam, Y. K.; Ciufolini, M.; Witzigmann, D.; Kulkarni, J. A.; van der Meel, R.; Cullis, P. R. The Onpattro story and the clinical translation of nanomedicines containing nucleic acid-based drugs. *Nat. Nanotechnol.* **2019**, *14*, 1084−1087.

(14) Balwani, M.; Sardh, E.; Ventura, P.; Peiró, P. A.; Rees, D. C.; Stölzel, U.; Bissell, D. M.; Bonkovsky, H. L.; Windyga, J.; Anderson, K. E.; Parker, C.; Silver, S. M.; Keel, S. B.; Wang, J.-D.; Stein, P. E.; Harper, P.; Vassiliou, D.; Wang, B.; Phillips, J.; Ivanova, A.; Langendonk, J. G.; Kauppinen, R.; Minder, E.; Horie, Y.; Penz, C.; Chen, J.; Liu, S.; Ko, J. J.; Sweetser, M. T.; Garg, P.; Vaishnaw, A.; Kim, J. B.; Simon, A. R.; Gouya, L. Phase 3 Trial of RNAi Therapeutic Givosiran for Acute Intermittent Porphyria. *N. Engl. J. Med.* **2020**, *382*, 2289−2301.

(15) Chan, A.; Liebow, A.; Yasuda, M.; Gan, L.; Racie, T.; Maier, M.; Kuchimanchi, S.; Foster, D.; Milstein, S.; Charisse, K.; Sehgal, A.; Manoharan, M.; Meyers, R.; Fitzgerald, K.; Simon, A.; Desnick, R. J.; Querbes, W. Preclinical Development of a Subcutaneous ALAS1 RNAi Therapeutic for Treatment of Hepatic Porphyrias Using Circulating RNA Quantification. *Mol. Ther.−Nucleic Acids* **2015**, *4*, No. e263.

(16) Liebow, A.; Li, X.; Racie, T.; Hettinger, J.; Bettencourt, B. R.; Najafian, N.; Haslett, P.; Fitzgerald, K.; Holmes, R. P.; Erbe, D.; Querbes, W.; Knight, J. An Investigational RNAi Therapeutic Targeting Glycolate Oxidase Reduces Oxalate Production in Models of Primary Hyperoxaluria. *JASN* **2017**, *28*, 494−503.

(17) Raal, F. J.; Kallend, D.; Ray, K. K.; Turner, T.; Koenig, W.; Wright, R. S.; Wijngaard, P. L. J.; Curcio, D.; Jaros, M. J.; Leiter, L. A.; Kastelein, J. J. P. Inclisiran for the Treatment of Heterozygous Familial Hypercholesterolemia. *N. Engl. J. Med.* **2020**, *382*, 1520−1530.

(18) Ray, K. K.; Wright, R. S.; Kallend, D.; Koenig, W.; Leiter, L. A.; Raal, F. J.; Bisch, J. A.; Richardson, T.; Jaros, M.; Wijngaard, P. L. J.; Kastelein, J. J. P. Two Phase 3 Trials of Inclisiran in Patients with Elevated LDL Cholesterol. *N. Engl. J. Med.* **2020**, *382*, 1507−1519.

(19) Fitzgerald, K.; White, S.; Borodovsky, A.; Bettencourt, B. R.; Strahs, A.; Clausen, V.; Wijngaard, P.; Horton, J. D.; Taubel, J.; Brooks, A.; Fernando, C.; Kauffman, R. S.; Kallend, D.; Vaishnaw, A.; Simon, A. A Highly Durable RNAi Therapeutic Inhibitor of PCSK9. *N. Engl. J. Med.* **2017**, *376*, 41−51.

(20) Nair, J. K.; Willoughby, J. L.; Chan, A.; Charisse, K.; Alam, M. R.; Wang, Q.; Hoekstra, M.; Kandasamy, P.; Kel'in, A. V.; Milstein, S.; Taneja, N.; O'Shea, J.; Shaikh, S.; Zhang, L.; van der Sluis, R. J.; Jung, M. E.; Akinc, A.; Hutabarat, R.; Kuchimanchi, S.; Fitzgerald, K.; Zimmermann, T.; van Berkel, T. J.; Maier, M. A.; Rajeev, K. G.; Manoharan, M. Multivalent N-acetylgalactosamine-conjugated siRNA localizes in hepatocytes and elicits robust RNAi-mediated gene silencing. *J. Am. Chem. Soc.* **2014**, *136*, 16958−16961.

(21) Egli, M.; Manoharan, M. Re-Engineering RNA Molecules into Therapeutic Agents. *Acc. Chem. Res.* **2019**, *52*, 1036−1047.

(22) O'Shea, J.; Theile, C. S.; Das, R.; Babu, I. R.; Charisse, K.; Manoharan, M.; Maier, M. A.; Zlatev, I. An efficient deprotection method for 5′-O,O-bis(pivaloyloxymethyl)-(E)-vinylphosphonate containing oligonucleotides. *Tetrahedron* **2018**, *74*, 6182−6186.

(23) Khvorova, A.; Watts, J. K. The chemical evolution of oligonucleotide therapies of clinical utility. *Nat. Biotechnol.* **2017**, *35*, 238−248.

(24) Pallan, P. S.; Greene, E. M.; Jicman, P. A.; Pandey, R. K.; Manoharan, M.; Rozners, E.; Egli, M. Unexpected origins of the enhanced pairing affinity of 2′-fluoro-modified RNA. *Nucleic Acids Res.* **2011**, *39*, 3482−3495.

(25) Kawasaki, A. M.; Casper, M. D.; Freier, S. M.; Lesnik, E. A.; Zounes, M. C.; Cummins, L. L.; Gonzalez, C.; Cook, P. D. Uniformly modified 2′-deoxy-2′-fluoro phosphorothioate oligonucleotides as nuclease-resistant antisense compounds with high affinity and specificity for RNA targets. *J. Med. Chem.* **1993**, *36*, 831−841.

(26) Schmit, C.; Bévierre, M.-O.; Mesmaeker, A. D.; Altmann, K.-H. The effects of 2′- and 3′-alkyl substituents on oligonucleotide hybridization and stability. *Bioorg. Med. Chem. Lett.* **1994**, *4*, 1969−1974.

(27) Cicero, D. O.; Mariana, G.; Philippe, J. N.; Adolfo, M. I. Synthesis and properties of (2′S)- and (2′R)-2′-deoxy-2′-C-methyl oligonucleotides. *Tetrahedron* **2001**, *57*, 7613−7621.

(28) Robaldo, L.; Izzo, F.; Dellafiore, M.; Proietti, C.; Elizalde, P. V.; Montserrat, J. M.; Iribarren, A. M. Influence of conformationally restricted pyrimidines on the activity of 10−23 DNAzymes. *Bioorg. Med. Chem.* **2012**, *20*, 2581−2586.

(29) Koole, L. H.; Wu, J. C.; Neidle, S.; Chattopadhyaya, J. Structural properties of four isomeric C2′/C3′ modified uridines. *J. Am. Chem. Soc.* **1992**, *114*, 2687−2696.

(30) Gamarnik, A.; Arnold, J. J.; Sharma, S. D.; Feng, J. Y.; Ray, A. S.; Smidansky, E. D.; Kireeva, M. L.; Cho, A.; Perry, J.; Vela, J. E.; Park, Y.; Xu, Y.; Tian, Y.; Babusis, D.; Barauskus, O.; Peterson, B. R.; Gnatt, A.; Kashlev, M.; Zhong, W.; Cameron, C. E. Sensitivity of Mitochondrial Transcription and Resistance of RNA Polymerase II Dependent Nuclear Transcription to Antiviral Ribonucleosides. *PLoS Pathog.* **2012**, *8*, No. e1003030.

(31) Reddy, P. G.; Bao, D.; Chang, W.; Chun, B.-K.; Du, J.; Nagarathnam, D.; Rachakonda, S.; Ross, B. S.; Zhang, H.-R.; Bansal, S.; Espiritu, C. L.; Keilman, M.; Lam, A. M.; Niu, C.; Steuer, H. M.; Furman, P. A.; Otto, M. J.; Sofia, M. J. 2′-Deoxy-2′-α-fluoro-2′-β-C-methyl 3′,5′-cyclic phosphate nucleotide prodrug analogs as inhibitors of HCV NS5B polymerase: Discovery of PSI-352938. *Bioorg. Med. Chem. Lett.* **2010**, *20*, 7376−7380.

(32) Zhou, S.; Mahmoud, S.; Liu, P.; Zhou, L.; Ehteshami, M.; Bassit, L.; Tao, S.; Domaoal, R. A.; Sari, O.; Schutter, C. D.; Amiralaei, S.; Khalil, A.; Ollinger Russell, O.; McBrayer, T.; Whitaker, T.; Abou-Taleb, N.; Amblard, F.; Coats, S. J.; Schinazi, R. F. 2′-Chloro,2′-fluoro Ribonucleotide Prodrugs with Potent Pan-genotypic

Activity against Hepatitis C Virus Replication in Culture. *J. Med. Chem.* **2017**, *60*, 5424−5437.

(33) Wang, P.; Chun, B. K.; Rachakonda, S.; Du, J.; Khan, N.; Shi, J.; Stec, W.; Cleary, D.; Ross, B. S.; Sofia, M. J. An efficient and diastereoselective synthesis of PSI-6130: a clinically efficacious inhibitor of HCV NS5B polymerase. *J. Org. Chem.* **2009**, *74*, 6819−6824.

(34) Sofia, M. J.; Bao, D.; Chang, W.; Du, J.; Nagarathnam, D.; Rachakonda, S.; Reddy, P. G.; Ross, B. S.; Wang, P.; Zhang, H. R.; Bansal, S.; Espiritu, C.; Keilman, M.; Lam, A. M.; Steuer, H. M.; Niu, C.; Otto, M. J.; Furman, P. A. Discovery of a β-d-2′-deoxy-2′-α-fluoro-2′-β-C-methyluridine nucleotide prodrug (PSI-7977) for the treatment of hepatitis C virus. *J. Med. Chem.* **2010**, *53*, 7202−7218.

(35) Chun, B. K.; Du, J.; Zhang, H. R.; Chang, W.; Ross, B. S.; Jiang, Y.; Bao, D.; Espiritu, C. L.; Keilman, M.; Steuer, H. M.; Furman, P. A.; Sofia, M. J. Synthesis of stable isotope labeled analogs of the anti-hepatitis C virus nucleotide prodrugs PSI-7977 and PSI-352938. *Nucleosides, Nucleotides Nucleic Acids* **2011**, *30*, 886−896.

(36) Ross, B. S.; Reddy, P. G.; Zhang, H. R.; Rachakonda, S.; Sofia, M. J. Synthesis of diastereomerically pure nucleotide phosphoramidates. *J. Org. Chem.* **2011**, *76*, 8311−8319.

(37) Du, J.; Bao, D.; Chun, B. K.; Jiang, Y.; Reddy, P. G.; Zhang, H. R.; Ross, B. S.; Bansal, S.; Bao, H.; Espiritu, C.; Lam, A. M.; Murakami, E.; Niu, C.; Micolochick Steuer, H. M.; Furman, P. A.; Otto, M. J.; Sofia, M. J. β-D-2′-α-F-2′-β-C-Methyl-6-O-substituted 3′,5′-cyclic phosphate nucleotide prodrugs as inhibitors of hepatitis C virus replication: a structure-activity relationship study. *Bioorg. Med. Chem. Lett.* **2012**, *22*, 5924−5929.

(38) Keating, G. M.; Vaidya, A. Sofosbuvir: first global approval. *Drugs* **2014**, *74*, 273−282.

(39) Feng, J. Y.; Xu, Y.; Barauskas, O.; Perry, J. K.; Ahmadyar, S.; Stepan, G.; Yu, H.; Babusis, D.; Park, Y.; McCutcheon, K.; Perron, M.; Schultz, B. E.; Sakowicz, R.; Ray, A. S. Role of Mitochondrial RNA Polymerase in the Toxicity of Nucleotide Inhibitors of Hepatitis C Virus. *Antimicrob. Agents Chemother.* **2016**, *60*, 806−817.

(40) Janas, M. M.; Zlatev, I.; Liu, J.; Jiang, Y.; Barros, S. A.; Sutherland, J. E.; Davis, W. P.; Liu, J.; Brown, C. R.; Liu, X.; Schlegel, M. K.; Blair, L.; Zhang, X.; Das, B.; Tran, C.; Aluri, K.; Li, J.; Agarwal, S.; Indrakanti, R.; Charisse, K.; Nair, J.; Matsuda, S.; Rajeev, K. G.; Zimmermann, T.; Sepp-Lorenzino, L.; Xu, Y.; Akinc, A.; Fitzgerald, K.; Vaishnaw, A. K.; Smith, P. F.; Manoharan, M.; Jadhav, V.; Wu, J. T.; Maier, M. A. Safety evaluation of 2′-deoxy-2′-fluoro nucleotides in GalNAc-siRNA conjugates. *Nucleic Acids Res.* **2019**, *47*, 3306−3320.

(41) Lima, W. F.; Prakash, T. P.; Murray, H. M.; Kinberger, G. A.; Li, W.; Chappell, A. E.; Li, C. S.; Murray, S. F.; Gaus, H.; Seth, P. P.; Swayze, E. E.; Crooke, S. T. Single-stranded siRNAs activate RNAi in animals. *Cell* **2012**, *150*, 883−894.

(42) Prakash, T. P.; Lima, W. F.; Murray, H. M.; Li, W.; Kinberger, G. A.; Chappell, A. E.; Gaus, H.; Seth, P. P.; Bhat, B.; Crooke, S. T.; Swayze, E. E. Identification of metabolically stable 5′-phosphate analogs that support single-stranded siRNA activity. *Nucleic Acids Res.* **2015**, *43*, 2993−3011.

(43) Parmar, R.; Willoughby, J. L.; Liu, J.; Foster, D. J.; Brigham, B.; Theile, C. S.; Charisse, K.; Akinc, A.; Guidry, E.; Pei, Y.; Strapps, W.; Cancilla, M.; Stanton, M. G.; Rajeev, K. G.; Sepp-Lorenzino, L.; Manoharan, M.; Meyers, R.; Maier, M. A.; Jadhav, V. 5′-(E)-Vinylphosphonate: A Stable Phosphate Mimic Can Improve the RNAi Activity of siRNA-GalNAc Conjugates. *ChemBioChem* **2016**, *17*, 985−989.

(44) Prakash, T. P.; Kinberger, G. A.; Murray, H. M.; Chappell, A.; Riney, S.; Graham, M. J.; Lima, W. F.; Swayze, E. E.; Seth, P. P. Synergistic effect of phosphorothioate, 5′-vinylphosphonate and GalNAc modifications for enhancing activity of synthetic siRNA. *Bioorg. Med. Chem. Lett.* **2016**, *26*, 2817−2820.

(45) Elkayam, E.; Parmar, R.; Brown, C. R.; Willoughby, J. L.; Theile, C. S.; Manoharan, M.; Joshua-Tor, L. siRNA carrying an (E)-vinylphosphonate moiety at the 5 end of the guide strand augments gene silencing by enhanced binding to human Argonaute-2. *Nucleic Acids Res.* **2017**, *45*, 3528−3536.

(46) Haraszti, R. A.; Roux, L.; Coles, A. H.; Turanov, A. A.; Alterman, J. F.; Echeverria, D.; Godinho, B.; Aronin, N.; Khvorova, A. 5′-Vinylphosphonate improves tissue accumulation and efficacy of conjugated siRNAs in vivo. *Nucleic Acids Res.* **2017**, *45*, 7581−7592.

(47) Parmar, R. G.; Brown, C. R.; Matsuda, S.; Willoughby, J. L. S.; Theile, C. S.; Charissé, K.; Foster, D. J.; Zlatev, I.; Jadhav, V.; Maier, M. A.; Egli, M.; Manoharan, M.; Rajeev, K. G. Facile Synthesis, Geometry, and 2′-Substituent-Dependent in Vivo Activity of 5′-(E)- and 5′-(Z)-Vinylphosphonate-Modified siRNA Conjugates. *J. Med. Chem.* **2018**, *61*, 734−744.

(48) Janas, M. M.; Schlegel, M. K.; Harbison, C. E.; Yilmaz, V. O.; Jiang, Y.; Parmar, R.; Zlatev, I.; Castoreno, A.; Xu, H.; Shulga-Morskaya, S.; Rajeev, K. G.; Manoharan, M.; Keirstead, N. D.; Maier, M. A.; Jadhav, V. Selection of GalNAc-conjugated siRNAs with limited off-target-driven rat hepatotoxicity. *Nat. Commun.* **2018**, *9*, No. 723.

(49) Snøve, O.; Rossi, J. J. Chemical Modifications Rescue Off-Target Effects of RNAi. *ACS Chem. Biol.* **2006**, *1*, 274−276.

(50) Bramsen, J. B.; Pakula, M. M.; Hansen, T. B.; Bus, C.; Langkjær, N.; Odadzic, D.; Smicius, R.; Wengel, S. L.; Chattopadhyaya, J.; Engels, J. W.; Herdewijn, P.; Wengel, J.; Kjems, J. A screen of chemical modifications identifies position-specific modification by UNA to most potently reduce siRNA off-target effects. *Nucleic Acids Res.* **2010**, *38*, 5761−5773.

(51) Mook, O. R.; Vreijling, J.; Wengel, S.; Wengel, J.; Zhou, C.; Chattopadhyaya, J.; Baas, F.; Fluiter, K. In vivo efficacy and off-target effects of Locked Nucleic Acid (LNA) and Unlocked Nucleic Acid (UNA) modified siRNA and small internally segmented interfering RNA (sisiRNA) in mice bearing human tumor xenografts. *Artif. DNA: PNA XNA* **2010**, *1*, 36−44.

(52) Laursen, M. B.; Pakula, M. M.; Gao, S.; Fluiter, K.; Mook, O. R.; Baas, F.; Langklær, N.; Wengel, S. L.; Wengel, J.; Kjems, J.; Bramsen, J. B. Utilization of unlocked nucleic acid (UNA) to enhance siRNA performance in vitro and in vivo. *Mol. BioSyst.* **2010**, *6*, 862−870.

(53) Vaish, N.; Chen, F.; Seth, S.; Fosnaugh, K.; Liu, Y.; Adami, R.; Brown, T.; Chen, Y.; Harvie, P.; Johns, R.; Severson, G.; Granger, B.; Charmley, P.; Houston, M.; Templin, M. V.; Polisky, B. Improved specificity of gene silencing by siRNAs containing unlocked nucleobase analogs. *Nucleic Acids Res.* **2011**, *39*, 1823−1832.

(54) Seok, H.; Lee, H.; Jang, E.-S.; Chi, S. W. Evaluation and control of miRNA-like off-target repression for RNA interference. *Cell. Mol. Life Sci.* **2018**, *75*, 797−814.

(55) Bartoszewski, R.; Sikorski, A. F. Editorial focus: understanding off-target effects as the key to successful RNAi therapy. *Cell. Mol. Biol. Lett.* **2019**, *24*, No. 69.

(56) Neumeier, J.; Meister, G. siRNA Specificity: RNAi Mechanisms and Strategies to Reduce Off-Target Effects. *Front. Plant Sci.* **2021**, *11*, No. 526455.

(57) Mergny, J. L.; Lacroix, L. Analysis of thermal melting curves. *Oligonucleotides* **2003**, *13*, 515−537.

(58) Bernardi, A.; Bernardi, G. Studies on acid hydrolases. IV. Isolation and characterization of spleen exonuclease. *Biochim. Biophys. Acta* **1968**, *155*, 360−370.

(59) Kenski, D. M.; Cooper, A. J.; Li, J. J.; Willingham, A. T.; Haringsma, H. J.; Young, T. A.; Kuklin, N. A.; Jones, J. J.; Cancilla, M. T.; McMasters, D. R.; Mathur, M.; Sachs, A. B.; Flanagan, W. M. Analysis of acyclic nucleoside modifications in siRNAs finds sensitivity at position 1 that is restored by 5′-terminal phosphorylation both in vitro and in vivo. *Nucleic Acids Res.* **2010**, *38*, 660−671.

(60) Elkayam, E.; Kuhn, C. D.; Tocilj, A.; Haase, A. D.; Greene, E. M.; Hannon, G. J.; Joshua-Tor, L. The structure of human argonaute-2 in complex with miR-20a. *Cell* **2012**, *150*, 100−110.

(61) Dobin, A.; Davis, C. A.; Schlesinger, F.; Drenkow, J.; Zaleski, C.; Jha, S.; Batut, P.; Chaisson, M.; Gingeras, T. R. STAR: ultrafast universal RNA-seq aligner. *Bioinformatics* **2013**, *29*, 15−21.

(62) Liao, Y.; Smyth, G. K.; Shi, W. featureCounts: an efficient general purpose program for assigning sequence reads to genomic features. *Bioinformatics* **2014**, *30*, 923−930.

(63) Love, M. I.; Huber, W.; Anders, S. Moderated estimation of fold change and dispersion for RNA-seq data with DESeq2. *Genome Biol.* **2014**, *15*, No. 550.

(64) Agarwal, V.; Bell, G. W.; Nam, J. W.; Bartel, D. P. Predicting effective microRNA target sites in mammalian mRNAs. *eLife* **2015**, *4*, No. e05005.

(65) Doench, J. G.; Petersen, C. P.; Sharp, P. A. siRNAs can function as miRNAs. *Genes Dev.* **2003**, *17*, 438−442.

(66) Ui-Tei, K.; Naito, Y.; Nishi, K.; Juni, A.; Saigo, K. Thermodynamic stability and Watson-Crick base pairing in the seed duplex are major determinants of the efficiency of the siRNA-based off-target effect. *Nucleic Acids Res.* **2008**, *36*, 7100−7109.

(67) Jayaraman, M.; Ansell, S. M.; Mui, B. L.; Tam, Y. K.; Chen, J.; Du, X.; Butler, D.; Eltepu, L.; Matsuda, S.; Narayanannair, J. K.; Rajeev, K. G.; Hafez, I. M.; Akinc, A.; Maier, M. A.; Tracy, M. A.; Cullis, P. R.; Madden, T. D.; Manoharan, M.; Hope, M. J. Maximizing the potency of siRNA lipid nanoparticles for hepatic gene silencing in vivo. *Angew. Chem., Int. Ed.* **2012**, *51*, 8529.

(68) Schlegel, M. K.; Foster, D. J.; Kel'in, A. V.; Zlatev, I.; Bisbe, A.; Jayaraman, M.; Lackey, J. G.; Rajeev, K. G.; Charissé, K.; Harp, J.; Pallan, P. S.; Maier, M. A.; Egli, M.; Manoharan, M. Chirality Dependent Potency Enhancement and Structural Impact of Glycol Nucleic Acid Modification on siRNA. *J. Am. Chem. Soc.* **2017**, *139*, 8537−8546.

(69) Clark, J. L.; Hollecker, L.; Mason, J. C.; Stuyver, L. J.; Tharnish, P. M.; Lostia, S.; McBrayer, T. R.; Schinazi, R. F.; Watanabe, K. A.; Otto, M. J.; Furman, P. A.; Stec, W. J.; Patterson, S. E.; Pankiewicz, K. W. Design, synthesis, and antiviral activity of 2′-deoxy-2′-fluoro-2′-C-methylcytidine, a potent inhibitor of hepatitis C virus replication. *J. Med. Chem.* **2005**, *48*, 5504−5508.

(70) Sofia, M. J.; Bao, D.; Chang, W.; Du, J.; Nagarathnam, D.; Rachakonda, S.; Reddy, P. G.; Ross, B. S.; Wang, P.; Zhang, H. R.; Bansal, S.; Espiritu, C.; Keilman, M.; Lam, A. M.; Steuer, H. M.; Niu, C.; Otto, M. J.; Furman, P. A. Discovery of a β-d-2′-deoxy-2′-α-fluoro-2′-β-C-methyluridine nucleotide prodrug (PSI-7977) for the treatment of hepatitis C virus. *J. Med. Chem.* **2010**, *53*, 7202−7218.

(71) Pettersen, E. F.; Goddard, T. D.; Huang, C. C.; Couch, G. S.; Greenblatt, D. M.; Meng, E. C.; Ferrin, T. E. UCSF Chimera−a visualization system for exploratory research and analysis. *J. Comput. Chem.* **2004**, *25*, 1605−1612.

(72) Pallan, P. S.; Greene, E. M.; Jicman, P. A.; Pandey, R. K.; Manoharan, M.; Rozners, E.; Egli, M. Unexpected origins of the enhanced pairing affinity of 2′-fluoro-modified RNA. *Nucleic Acids Res.* **2011**, *39*, 3482−3495.

(73) Jinek, M.; Coyle, S. M.; Doudna, J. A. Coupled 5′ nucleotide recognition and processivity in Xrn1-mediated mRNA decay. *Mol. Cell* **2011**, *41*, 600−608.

(74) Brautigam, C. A.; Steitz, T. A. Structural principles for the inhibition of the 3′-5′ exonuclease activity of Escherichia coli DNA polymerase I by phosphorothioates. *J. Mol. Biol.* **1998**, *277*, 363−377.

(75) Akabane-Nakata, M.; Erande, N. D.; Kumar, P.; Degaonkar, R.; Gilbert, J. A.; Qin, J.; Mendez, M.; Woods, L. B.; Jiang, Y.; Janas, M. M.; O'Flaherty, D. K.; Zlatev, I.; Schlegel, M. K.; Matsuda, S.; Egli, M.; Manoharan, M. siRNAs containing 2′-fluorinated Northern-methanocarbacyclic (2′-F-NMC) nucleotides: in vitro and in vivo RNAi activity and inability of mitochondrial polymerases to incorporate 2′-F-NMC NTPs. *Nucleic Acids Res.* **2021**, *49*, 2435−2449.

(76) Szymanski, M. R.; Kuznetsov, V. B.; Shumate, C.; Meng, Q.; Lee, Y. S.; Patel, G.; Patel, S.; Yin, Y. W. Structural basis for processivity and antiviral drug toxicity in human mitochondrial DNA replicase. *EMBO J.* **2015**, *34*, 1959−1970.

(77) Schirle, N. T.; Sheu-Gruttadauria, J.; MacRae, I. J. Structural basis for microRNA targeting. *Science* **2014**, *346*, 608−613.

(78) Arnold, J. J.; Smidansky, E. D.; Moustafa, I. M.; Cameron, C. E. Human mitochondrial RNA polymerase: structure-function, mecha-nism and inhibition. *Biochim. Biophys. Acta, Gene Regul. Mech.* **2012**, *1819*, 948−960.

(79) Manoharan, M.; Akinc, A.; Pandey, R. K.; Qin, J.; Hadwiger, P.; John, M.; Mills, K.; Charisse, K.; Maier, M. A.; Nechev, L.; Greene, E. M.; Pallan, P. S.; Rozners, E.; Rajeev, K. G.; Egli, M. Unique Gene-Silencing and Structural Properties of 2′-Fluoro-Modified siRNAs. *Angew. Chem., Int. Ed.* **2011**, *50*, 2284−2288.

(80) Reddy, P. G.; Bao, D.; Chang, W.; Chun, B. K.; Du, J.; Nagarathnam, D.; Rachakonda, S.; Ross, B. S.; Zhang, H. R.; Bansal, S.; Espiritu, C. L.; Keilman, M.; Lam, A. M.; Niu, C.; Steuer, H. M.; Furman, P. A.; Otto, M. J.; Sofia, M. J. 2′-deoxy-2′-α-fluoro-2′-β-C-methyl 3′,5′-cyclic phosphate nucleotide prodrug analogs as inhibitors of HCV NS5B polymerase: discovery of PSI-352938. *Bioorg. Med. Chem. Lett.* **2010**, *20*, 7376−7380.

(81) Chang, W.; Bao, D.; Chun, B. K.; Naduthambi, D.; Nagarathnam, D.; Rachakonda, S.; Reddy, P. G.; Ross, B. S.; Zhang, H. R.; Bansal, S.; Espiritu, C. L.; Keilman, M.; Lam, A. M.; Niu, C.; Steuer, H. M.; Furman, P. A.; Otto, M. J.; Sofia, M. J. Discovery of PSI-353661, a Novel Purine Nucleotide Prodrug for the Treatment of HCV Infection. *ACS Med. Chem. Lett.* **2011**, *2*, 130−135.

(82) Reddy, P. G.; Chun, B. K.; Zhang, H. R.; Rachakonda, S.; Ross, B. S.; Sofia, M. J. Stereoselective synthesis of PSI-352938: a β-D-2′-deoxy-2′-α-fluoro-2′-β-C-methyl-3′,5′-cyclic phosphate nucleotide prodrug for the treatment of HCV. *J. Org. Chem.* **2011**, *76*, 3782−3790.

▢ Recommended by ACS